HIGH-EFFICIENCY AMORPHOUS SILICON ALLOY BASED SOLAR CELLS AND MODULES

Annual Technical Progress Report
June 1, 2003 through May 31, 2004

S. Guha and J. Yang
United Solar Ovonic Corporation
Troy, Michigan

NREL Technical Monitor: Bolko von Roedern

Prepared under Subcontract No. ZDJ-2-30630-19

Preface

This annual Subcontract Report covers the work performed by United Solar Ovonic Corporation for the period from June 1, 2003 to May 31, 2004 under NREL thin film partnership Subcontract No. ZDJ-2-30630-19. The following personnel participated in this research program.

A. Banerjee, E. Chen, G. Fischer, G. Ganguly, S. Guha (Principal Investigator), B. Hang, M. Hopson, N. Jackett, K. Lord, A. Mohsin, T. Nazmee, J. Noch, J. M. Owens, T. Palmer, G. Pietka, D. Wolf, B. Yan, J. Yang (Co-Principal Investigator), K. Younan, and G. Yue.

Collaboration with the Colorado School of Mines, University of North Carolina, University of Oregon, Syracuse University, and the National Renewable Energy Laboratory is acknowledged. We would like to thank S. R. Ovshinsky and H. Fritzsche for their constant encouragement and useful discussion, and S. Sundquist for preparation of this report.

Executive Summary

Objectives

The principal objective of this R&D program is to expand, enhance, and accelerate knowledge and capabilities for development of high efficiency hydrogenated amorphous silicon (a-Si:H) and amorphous silicon-germanium alloy (a-SiGe:H) related thin film multi-junction solar cells and modules with low manufacturing cost and high reliability. Our strategy has been to use the spectrum-splitting triple-junction structure, a-Si:H/a-SiGe:H/a-SiGe:H, to improve solar cell and module efficiency, stability, and throughput of production. The methodology used to achieve the objectives included: i) explore the highest stable efficiency using the triple-junction structure deposited using RF glow discharge at a low rate, ii) fabricate the devices at a high deposition rate for high throughput and low cost, and iii) develop optimized recipe using the R&D batch large-area reactor to help the design and optimization of the production roll-to-roll machines. In the last few years, the research on hydrogenated nanocrystalline silicon (nc-Si:H) solar cells has attracted significant attention in Japan and Europe. Using nc-Si:H as the bottom cell in multi-junction structures, cell efficiency of over 14% and module efficiency of over 13% have been reported. We have been exploring the use of nc-Si:H as an intrinsic layer of the bottom cell in the triple-junction solar cell to achieve higher stable cell and module efficiency. During the past year, we have worked on developing high efficiency nc-Si:H single-junction solar cells and high efficiency multi-junction solar cells using nc-Si:H as the intrinsic layer of the bottom cell. We have achieved an initial active-area efficiency of 14.6% using an a-Si:H/a-SiGe:H/nc-Si:H triple-junction structure.

Approach

In manufacturing, United Solar uses a triple-junction spectral-splitting solar cell structure and a roll-to-roll deposition process. The conventional a-Si:H/a-SiGe:H/a-SiGe:H triple-junction cells use an a-Si:H top cell (~1.8 eV bandgap) to absorb the blue light, an a-SiGe:H middle cell with ~20% germanium (~1.6 eV bandgap) to absorb the green light, and an a-SiGe:H bottom cell with ~40% germanium (~1.4 eV bandgap) to capture the red light. One objective of this program is to continue the optimization of a-SiGe:H middle and bottom cells to achieve high efficiency. At the same time, we are developing nc-Si:H solar cells as a potential replacement of the a-SiGe:H bottom cell in the triple-junction structures. During the past year, we continued to work on the optimization of nc-Si:H single-junction solar cells at various deposition rates and incorporated the improved nc-Si:H single-junction cell in a-Si:H/nc-Si:H double-junction and a-Si:H/a-SiGe:H/nc-Si:H triple-junction structures. Another objective is to work on the issues of large-area deposition using the a-Si:H/a-SiGe:H/a-SiGe:H triple-junction structure. Last year, we modified the "2B" machine (this is a multi-chamber R&D deposition machine that can use substrates of area 15" x 14") by replacing the existing deposition cathodes with modified cathodes in order to improve the uniformity and cell efficiency. The new cathode design is similar to that used in our current 30 MW/year production machine. Any gain in cell efficiency obtained in the 2B machine can be transferred to the production equipment. In the past year, we used the improved hardware design to optimize a-Si:H/a-SiGe:H/a-SiGe:H triple-junction cells using the 30 MW/year production constraints. Meanwhile, we have also been testing the feasibility of deposition of a-Si:H/nc-Si:H double-junction cells on large-area substrates and fabrication of modules.

In order to meet the program objectives, we have carried out research in the following areas: i) deposition of nc-Si:H films and solar cells using RF glow discharge at a low rate ~1 Å/s to achieve the highest efficiency, ii) deposition of nc-Si:H films and solar cells using MVHF glow discharge at a high rate of ~3-10 Å/s, iii) deposition of nc-Si:H films and solar cells using RF glow discharge under a high pressure depleting regime at a high rate of ~3-5 Å/s, iv) deposition of a-Si:H/nc-SiGe:H double-junction solar cells on large-area substrates using the 2B machine, v) deposition of a-Si:H/a-SiGe:H/a-Si:H triple-junction solar cells on large-area substrates using the constraints of the 30 MW/year production machine, vi) metastability of nc-Si:H single-junction, a-Si:H/nc-Si:H double-junction, and a-Si:H/a-SiGe:H/nc-Si:H and a-Si:H/a-SiGe:H/a-SiGe:H triple-junction solar cells. In addition, we collaborated with the Colorado School of Mines, University of North Carolina, University of Oregon, Syracuse University, and NREL on material and solar cell characterizations.

Status/Accomplishments

Small-area cells deposited using RF glow discharge at low rates

We have worked on developing and optimizing nc-Si:H materials and solar cells using RF glow discharge at low rates to search for the highest efficiency with different cell structures. The highest efficiency values achieved are listed below. We give values for active-area efficiency. The grid loss is typically ~7%, and the total area efficiency is therefore ~7% lower.

- 8.4% initial active-area (0.25 cm^2) cell efficiency in a nc-Si:H single-junction structure.
- 13.5% initial and 11.8% stable active-area (0.25 cm^2) cell efficiencies in an a-Si:H/nc-Si:H double-junction structure.
- 14.6% initial active-area (0.25 cm^2) cell efficiency in an a-Si:H/a-SiGe:H/nc-Si:H triple-junction structure. Light soaking experiment on this solar cell is under way.

Small-area cells deposited using MVHF glow discharge at high rates

We have used a modified very-high-frequency (MVHF) glow discharge to deposit nc-Si:H material and solar cells at high deposition rates ~ 3-10 Å/s using parameters that satisfy production requirements. We have achieved the following results in this deposition regime.

- An initial active-area (0.25 cm^2) efficiency of 7.7% has been achieved using nc-Si:H single-junction cell made at high rates.
- An initial active-area (0.25 cm^2) efficiency of 12.5% has been achieved using a-Si:H/nc-Si:H double-junction cell made at high rates. The cell efficiency stabilized at 11.0% after prolonged light soaking.
- An initial active-area (0.25 cm^2) efficiency of 12.8% has been achieved using a-Si:H/a-SiGe:H/nc-Si:H triple-junction cell made at high rates. The cell efficiency stabilized at 11.4% after prolonged light soaking.

Small-area cells deposited using RF glow discharge under high pressure at high deposition rates

We have used RF glow discharge under high pressure with high power to obtain high rate deposition of nc-Si:H solar cells. The current deposition rate is in the range of 3-5 Å/s. The following results have been achieved using this method.

- An initial active-area (0.25 cm^2) efficiency of 6.7% has been achieved using nc-Si:H single-junction cell.
- An initial active-area (0.25 cm^2) efficiency of 12.3% has been achieved using a-Si:H/nc-Si:H double-junction cell.

Large-area (2B machine) deposition of a-Si:H/nc-Si:H double-junction solar cells

- An initial active-area (0.25 cm^2) efficiency of 12.1% has been achieved using a-Si:H/nc-Si:H double-junction cell at a low rate ~ 1 Å/s. A stable active-area efficiency of 11.0% has also been achieved.
- An initial aperture-area (45 cm^2) efficiency of 11.8% has been achieved using an a-Si:H/nc-Si:H double-junction cell at a low rate ~ 1 Å/s. The stable cell efficiency is 10.3%.
- An initial aperture-area (460 cm^2) efficiency of 11.3% has been achieved in a-Si:H/μc-Si:H double-junction cell deposited at a low rate ~ 1 Å/s. The cell efficiency became 10.5% after encapsulation and stabilized at 9.4% after prolonged light soaking. NREL measured an efficiency of 9.2%.

Large-area (2B machine) deposition of a-Si:H/a-SiGe:H/a-SiGe:H triple-junction solar cells using the constraints of the 30 MW/year production line

- An initial active-area (0.25 cm^2) efficiency of 11.4% was achieved using a-Si:H/a-SiGe:H/a-SiGe:H triple-junction cell deposited on a large-area Al/ZnO back reflector from the production line. The deposition conditions were under production constraints of using SiH_4 and GeH_4 instead of Si_2H_6 and GeH_4 for the gas mixture. A stable active-area efficiency of 9.8% was achieved. This value corresponds to a stable total-area efficiency of 9.1%, and is the same as our best value achieved with a Si_2H_6 and GeH_4 mixture at high rates.

Stability of single-junction and multi-junction solar cells with nc-Si:H in the bottom cell

We have systematically studied the light-induced degradation in nc-Si:H single-junction and multi-junction cells using nc-Si:H in the bottom cell. The following is a list of the key results.

- A light-induced degradation in nc-Si:H single-junction cell efficiency was found to be in the range of 7% to 20% depending on the deposition conditions and cell structure.
- The light-induced degradation occurs mainly in the amorphous phase.
- A bottom cell limited current mismatching improves the stable efficiency.

Publications

1. Subhendu Guha, Jeffrey Yang, Arindam Banerjee, Baojie Yan, and Kenneth Lord, "High quality amorphous silicon materials and cells grown with hydrogen dilution", *Solar Energy Materials & Solar Cells* **78**, 329 (2003).

2. Jeffrey Yang, Arindam Banerjee, and Subhendu Guha, "Amorphous silicon based photovoltaic-from earth to the "final frontier"", *Solar Energy Materials & Solar Cells* **78**, 597 (2003).

3. Andrea Hilchey, Chris Lawyer, Keda Wang, Daxing Han, Baojie Yan, Guozhen Yue, Jeffrey Yang, and Subhendu Guha, "Buffer-layer Effect on mixed-phase cells studied by micro-Raman and photoluminescence spectroscopy", *Mater. Res. Soc. Symp. Proc.* **808***,* A4.38 (2004).

4. Subhendu Guha, "Amorphous and microcrystalline silicon based photovoltaic", *Mater. Res. Soc. Symp. Proc.* **808***,* A6.4 (2004).

5. Baojie Yan, Guozhen Yue, Jeffrey Yang, Subhendu Guha, D. L. Williamson, D. Han, and C.-S. Jiang, "Microstructure evolution with thickness and hydrogen dilution profile in microcrystalline silicon solar cells", *Mater. Res. Soc. Symp. Proc.* **808***,* A8.5 (2004).

6. James J. Gutierrez, Adam F. Halverson, Eric D. Tweeten, J. David Cohen, Baojie Yan, Jeffrey Yang, and Subhendu Guha, "Electronic properties of RF glow discharge intrinsic microcrystalline silicon near the amorphous silicon phase boundary", *Mater. Res. Soc. Symp. Proc.* **808***,* A8.9 (2004).

7. Baojie Yan, Guozhen Yue, Arindam Banerjee, Jeffrey Yang, and Subhendu Guha, " Large-area hydrogenated amorphous and microcrystalline silicon double-junction solar cells", *Mater. Res. Soc. Symp. Proc.* **808***,* A9.41 (2004).

8. C.-S. Jiang, H.R. Moutinho, Q. Wang, M.M. Al-Jassim, B. Yan, J. Yang, and S. Guha, " Measurement of electric potential on amorphous silicon and amorphous silicon germanium alloy thin-film solar cells by scanning Kelvin probe microscopy", *Mater. Res. Soc. Symp. Proc.* **808***,* A9.42 (2004).

9. Guozhen Yue, Baojie Yan, Jessica M. Owens, Jeffrey Yang, and Subhendu Guha, "Microcrystalline silicon solar cells deposited using modified very-high frequency glow discharge and its application in multi-junction structures", *Mater. Res. Soc. Symp. Proc.* **808***,* A9.43 (2004).

10. Yueqin Xu, Baojie Yan, Brent P. Nelson, Eugene Iwaniczko, Robert C. Reedy, A.H. Mahan, and Howard Branz, "Devices fabrication with narrow-bandgap a-SiGe:H alloys deposited by HWCVD", *Mater. Res. Soc. Symp. Proc.* **808***,* A9.51 (2004).

11. Keda Wang, Anthony Canning, J.R.Weinberg-Wolf, E.C.T. Harley, Daxing Han, Baojie Yan, Guozhen Yue, Jeffrey Yang, and Subhendu Guha, "Correlation of hydrogenated nanocrystalline silicon microstructure and solar cell performance" *Mater. Res. Soc. Symp. Proc.* **808***,* A9.53 (2004).

12. Baojie Yan, Guozhen Yue, Jeffrey Yang, Subhendu Guha, D.L. Williamson, Daxing Han, and Chun-Sheng Jiang, "Hydrogen dilution profiling for hydrogenated microcrystalline silicon solar cells", to be published in *Appl. Phys. Lett.* (2004).

13. Baojie Yan, Guozhen Yue, Jessica M. Owens, Jeffrey Yang, and Subhendu Guha, "Light-induced metastability in hydrogenated nanocrystalline silicon solar cells", to be published in *Appl. Phys. Lett.* (2004).

14. S. O. Kasap, M. Gunes, R. E. Johanson, Q. Wang, J. Yang, and S. Guha, "Conductance Fluctuations in a-Si:H: effects of alloying and device structure", *J. Mat. Science: Materials in Electronics* **14**, 693 (2003).

Section 1: Introduction

This report covers Phase II of the program. As reported previously, we have expanded our research scope from traditional a-Si:H/a-SiGe:H/a-SiGe:H triple-junction solar cells to multi-junction structures with nc-Si:H as the bottom cell. We have previously achieved world record stable cell efficiency of 13% and a module efficiency of 10.5% using the a-Si:H/a-SiGe:H/a-SiGe:H triple-junction structure. This technology has been successfully transferred to our 30 MW/year capacity plant at Auburn Hills, Michigan. The main objective of the current R&D research program is to address the Department of Energy (DOE) goal of attaining 15% thin film module efficiency by developing new materials, device designs, and low cost manufacturing processes. At the same time, the research program provides support for improving the cell efficiency and reducing production cost. In the past, we focused on a-Si:H and a-SiGe:H alloy based solar cells. The a-Si:H/a-SiGe:H/a-SiGe:H triple-junction structure is currently the frontrunner for obtaining the highest stable cell efficiency. Recently, nc-Si:H solar cells have emerged as a potential substitute for the middle and bottom cells in the multi-junction structure due to low light-induced degradation and no GeH_4 needed in the deposition process. For comparison, Kaneka Corp. [1] has reported over 14% initial cell efficiency using an a-Si:H/nc-Si:H double-junction structure and Canon, Inc. [2] achieved an over 13% initial a-Si:H/nc-Si:H/nc-Si:H triple-junction module efficiency.

We have also worked on the development of nc-Si:H solar cells with the objective of using the nc-Si:H layer as the bottom intrinsic layer in a multi-junction structure [3]. We have carried out deposition of nc-Si:H materials and solar cells using conventional RF glow discharge at a low rate ~1 Å/s to explore the practical limits of achievable efficiency.

Due to the indirect-bandgap, the absorption coefficients are lower in nc-Si:H than in a-SiGe:H. A relatively thick intrinsic nc-Si:H is needed to generate sufficient photocurrent. Therefore, a high rate deposition is essential for nc-Si:H solar cell in production. We have worked on the modified very high frequency (MVHF) technique at high deposition rates of ~3-10 Å/s to develop technology that is compatible with production. In a parallel effort, we also tried to use RF glow discharge in a high pressure depleting regime for high rate nc-Si:H deposition. Since both the MVHF and high pressure RF glow discharge may have potential problems in production in terms of achievable deposition rate with acceptable efficiency, uniformity, and powder formation, a comparative study is necessary for evaluating the feasibility of each technology for mass production.

Since nc-Si:H has unique properties in terms of cell performance and deposition process, we need to investigate possible issues such as uniformity and compatibility with the roll-to-roll technology to incorporate nc-Si:H in multi-junction cells for production. During this year, we studied the deposition of a-Si:H/nc-Si:H double-junction solar cells on large area substrates and tested the compatibility of procedures for module fabrication.

a-Si:H and a-SiGe:H alloys are still the materials used in the current 30 MW/year production line. Improving a-SiGe:H middle and bottom cells further becomes necessary, because any improvement either in the efficiency and stability or deposition rate will lead to the reduction of production cost. Last year, we redesigned new cathodes for the 2B machine taking into account the constraints of the production machine. Since the new hardware was installed in the machine, the uniformity has improved. During this past year, we have optimized a-Si:H and

a-SiGe:H component cells as well as the a-Si:H/a-SiGe:H/a-SiGe:H triple-junction structure on this modified machine.

nc-Si:H solar cells have been reported to exhibit no light-induced degradation. However, the term nc-Si:H represents a wide spectrum of materials with various grain sizes and different crystalline volume fractions. Therefore, one expects different stability behaviors in nc-Si:H solar cells with different microstructures. In addition, in an a-Si:H/nc-Si:H double-junction structure, the top cell is usually an a-Si:H cell with relatively thick intrinsic layer to generate enough current for current matching with the nc-Si:H bottom cell. A thick a-Si:H cell might lead to a poor overall stability. Therefore, the stability study of nc-Si:H solar cells is an interesting topic not only for the fundamental understanding of the material, but also for the optimized design of stable multi-junction solar cells. Over the past year, we have systematically studied the light-induced degradation in various nc-Si:H cells and under various conditions.

Section 2: Optimization of nc-Si:H Solar Cells

2.1. Introduction

One of the objectives of the program is to explore the highest achievable efficiency using a-Si:H based thin film solar cell technology. To date, the highest stable efficiency of 13% has been achieved using an a-Si:H/a-SiGe:H/a-SiGe:H triple-junction structure. In order to improve the cell efficiency further, we need constant effort to search for high quality a-Si:H and a-SiGe:H materials. In the meantime, we need to find an alternative material to low bandgap a-SiGe:H since a-SiGe:H has a higher defect density than a-Si:H. nc-Si:H was found to be a potential substitute for the a-SiGe:H bottom cell since it offers a better stability under prolonged illumination than a-SiGe:H [4]. The bandgap of nc-Si:H with high crystalline volume fraction (f_c) is normally close to 1.1 eV, which is the same value as crystalline silicon. Therefore, nc-Si:H solar cells generally have higher short-circuit current density (J_{sc}), but lower open-circuit voltage (V_{oc}) than a-Si:H and a-SiGe:H cells. Due to the nature of the indirect optical transition in this material, a relative thick intrinsic nc-Si:H layer is required for obtaining a high J_{sc}. Normally, the intrinsic nc-Si:H layer in an *nip* structure is over 1 μm thick, and sometimes it needs to be a few μm thick. In general, J_{sc} increases with intrinsic layer thickness in a given range. For a particular nc-Si:H solar cell, it has been reported that the intrinsic nc-Si:H layer was as thick as 4-5 μm thick. However, we find that J_{sc} reaches a maximum around 22-24 mA/cm^2 with a thickness in the range between 1 and 2 μm under our current deposition conditions. Increasing the thickness further leads to a decrease in J_{sc}, caused by a reduction of spectral response in the long wavelength region. Two mechanisms could be responsible for the low J_{sc} for thick nc-Si:H solar cells. One possibility is microcrystallite collision due to the textured substrate [5][6]. It has been reported that grains in the nc-Si:H films deposited on a textured substrate grow perpendicular to the local substrate surface and collide with each other when the film exceeds a certain thickness. Thus, microcrystallite collision results in a high defect density at the grain boundaries and, therefore, low cell performance. A second possible mechanism is the increase of f_c and grain size with film thickness. A value of f_c that is too high could cause poor grain boundary passivation, high microvoid density, and poor cell performance [7][8].

Over the course of this past year, we have systematically studied the thickness dependence of nc-Si:H material and the cell performance. In collaboration with Professor Daxing Han at University of North Carolina at Chapel Hill, Professor Don Williamson at Colorado School of Mines, and Dr. Chun-Sheng Jiang at National Renewable Energy Laboratory, we carried out the structure studies using Raman, Photoluminescence, X-ray diffraction, Small Angle x-ray Spectroscopy (SAXS), and Atomic Force Microcopy (AFM). We find that a significant increase of f_c and the grain size are responsible for the deterioration of cell efficiency. Based on the material property analysis, we have developed a method to control the evolution of the microstructures with thickness. We used Hydrogen Dilution Profiling Technique (HDPT) and improved nc-Si:H performance significantly.

We have used various deposition techniques for nc-Si:H solar cell deposition at different deposition rates. Since the material properties and cell performance for nc-Si:H solar cells deposited with different techniques have some commonalties, experience developed using a given deposition technique is easily transferred to another. Here, we present results of the optimization of nc-Si:H solar cells deposited using both RF and MVHF glow discharge techniques.

2.2. Thickness dependence of nc-Si:H solar cell performance

Here, we present thickness dependence of nc-Si:H cell performance as a function of the intrinsic layer thickness. Two sets of nc-Si:H single-junction solar cells were made using MVHF glow discharge with different intrinsic layer thicknesses. One set was made on textured Ag/ZnO coated stainless steel (BR), and another on specular stainless steel (SS). The same growth recipe was used for both sets of solar cells on two different substrates. The thickness of the samples was obtained using an optical method. The thickness showed a linear dependence on deposition time and confirmed a constant deposition rate. We found that the deposition rates are the same on SS and BR. The reason for comparing nc-Si:H cells deposited on SS and BR is that on a flat substrate (SS), the cell performance would not have the problem of crystallite collision that is expected to happen on textured BR. Thus, we can expect less deterioration of cell performance with increase of thickness.

Table I lists the J-V characteristics of nc-Si:H solar cells deposited on BR substrate with different intrinsic layer thickness. One can see that the J_{sc}, calibrated by quantum efficiency measurement, increases with increasing thickness up to 1.0 μm and then saturates. For the cell with a thickness around 2 μm, J_{sc} is actually *lower* than that of the cell with a thickness around 1 μm. As is usually observed, both the V_{oc} and FF decrease monotonically with increasing thickness. The overall cell efficiency reaches a maximum with a thickness around 1 μm. Figure 1 (a) plots the quantum efficiency (QE) of the six cells. One can see that for cells with a thin nc-Si:H intrinsic layer, the long wavelength response increases with cell thickness; but for the cell with a thick intrinsic layer around 2 μm, the response at the middle and long wavelength region is lower than the 1 μm thick cells. The remarkable increase of quantum efficiency under reverse bias indicates an insufficient collection, which can be related to excess recombination through defects in the intrinsic layer.

Table II lists the J-V characteristics of the nc-Si:H solar cells made with the same recipe as the corresponding cells deposited on BR, which are listed in Table I. One can see that the behaviors of the V_{oc} and FF versus thickness are similar for cells on SS as those on BR, but that J_{sc} keeps increasing up to the thickness of ~ 2 μm. Moreover, compared to cells of the same thickness on BR, the cells on SS have smaller J_{sc} and V_{oc}, but higher FF. From Fig. 1 (b), one

Table I. J-V characteristics of nc-Si:H cells deposited using MVHF on BR with different thicknesses, where FF_b and FF_r represent respectively the fill factor under blue and red light.

Run No.	Thickness (nm)	J_{sc} (mA/cm^2)	V_{oc} (V)	FF	P_{max} (mW/cm^2)	FF_b	FF_r
12116	290	16.41	0.503	0.638	5.27	0.620	0.610
12120	490	19.77	0.476	0.633	5.96	0.626	0.636
12121	940	23.25	0.443	0.585	6.03	0.617	0.620
12119	990	22.47	0.436	0.612	6.00	0.628	0.619
12122	1340	23.23	0.424	0.533	5.25	0.568	0.597
12124	1930	21.80	0.392	0.491	4.20	0.521	0.569

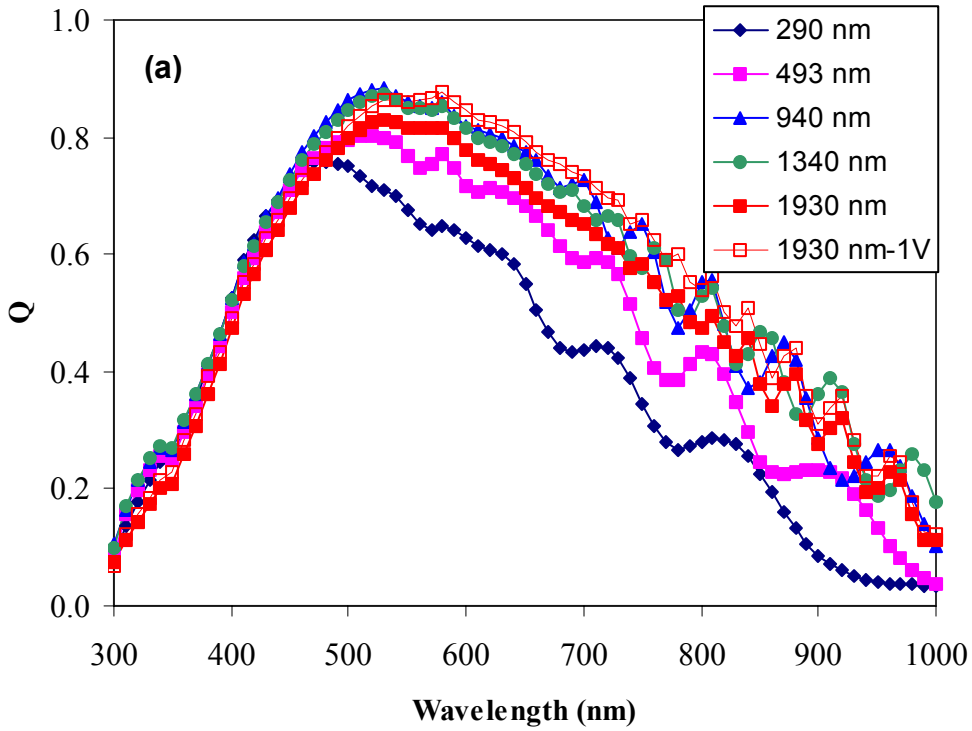

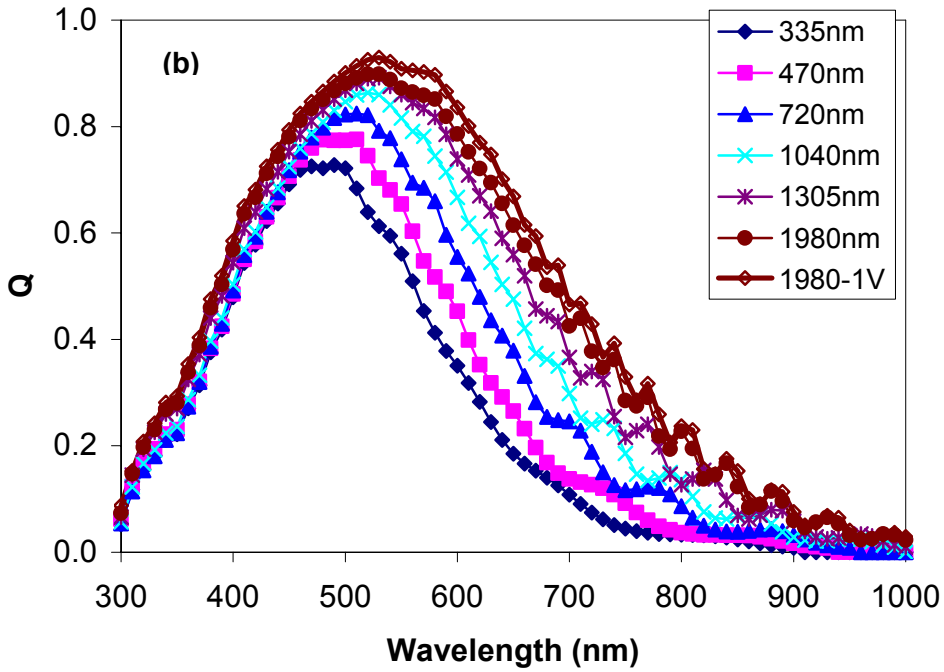

Figure 1. Quantum efficiency of nc-Si:H cells deposited using MVHF on (a) BR and on (b) SS with different thicknesses.

Table II. J-V characteristics of nc-Si:H solar cells deposited using MVHF on SS with different thicknesses, where FF_b and FF_r represent respectively the fill factor under blue and red light.

Run No.	Thickness (nm)	Q (mA/cm^2)	V_{oc} (V)	FF	P_{max} (mW/cm^2)	FF_b	FF_r
12129	335	9.45	0.47	0.651	2.89	0.650	0.668
12125	470	10.98	0.466	0.672	3.44	0.664	0.67
12127	720	12.99	0.439	0.64	3.65	0.608	0.627
12123	1040	14.8	0.434	0.621	3.99	0.649	0.655
12128	1305	16.51	0.414	0.578	3.95	0.615	0.632
12126	1980	17.87	0.393	0.51	3.58	0.584	0.612

can see the continued increase of the long wavelength response with thickness. The difference between the reverse biased quantum efficiency and the quantum efficiency under the short-circuit condition is much smaller for the 2 μm cell on SS than on BR. This implies that the cell on SS has less problems with carrier collection than on BR.

Due to the low reflectance and low light trapping effect from the specular SS substrate, the light absorption of the cells on SS is much less than that on BR for cells with the same thickness. This leads to a smaller J_{sc}, which causes a narrower quasi-Fermi level splitting and gives rise to a lower V_{oc}. Furthermore, the narrower quasi-Fermi level splitting reduces the recombination rate of the excited carriers, which yields a higher FF for cells on SS and hence, a lesser difference between the zero and negative biased quantum efficiency. A fair comparison of V_{oc} and FF for cells on different substrates would be under similar J_{sc}, instead of under the same light intensity. In this case, we may expect a similar splitting of the quasi-Fermi levels. For this purpose, the solar cells on BR were re-measured with reduced light intensities by using neutral density filters to generate similar current densities in the solar cells on SS. Table III lists J-V characteristics of four pairs of solar cells with different thicknesses. The two cells in each pair have a similar thickness, but one is on BR and the other on SS. One can see that when the solar cells on BR were adjusted to have J_{sc}'s similar to those on SS, the V_{oc} and FF also become very similar. This indicates that the BR substrate used at our lab does not have a pronounced effect on the carrier transport in the nc-Si:H solar cell. In conclusion, we found that the

Table III. Comparison of the solar cell performances with different substrates. For the measurements of the solar cells on BR, the light intensity was adjusted to have a J_{sc} similar to the solar cells on SS using neutral filters.

Thickness (nm)	Substrate	J_{sc} (mA/cm^2)	V_{oc} (V)	FF	P_{max} (mW/cm^2)
470	BR	11.7	0.451	0.646	3.42
	SS	11.8	0.467	0.669	3.69
1040	BR	15.4	0.421	0.636	4.12
	SS	15.6	0.435	0.623	4.22
1305	BR	17.0	0.413	0.551	3.88
	SS	17.5	0.416	0.579	4.22
1980	BR	18.7	0.385	0.501	3.61
	SS	18.8	0.395	0.508	3.76

microcrystallite collision for cells on BR could be a limitation of low J_{sc}, but it is not the main factor. Therefore, the other mechanism, which is the increase of crystalline volume fraction, could be responsible for the low J_{sc} in the thicker nc-Si:H solar cells.

2.3. Microstructure changes in nc-Si:H solar cells with thickness

As shown in the previous section, the evolution of crystallinity with thickness is probably the dominant contribution for the deterioration of cell performance with intrinsic layer thickness in our nc-Si:H solar cells. Although the collision of nanocrystallites may be present to some extent in the *nip* type cells on the textured Ag/ZnO back BR, it is not the limiting factor. The increase of crystalline volume fraction and grain size has been very well documented in the literature [9][10]. However, the properties of nc-Si:H material depend on deposition conditions and cells structures. In order to understand the increase of crystalline volume fraction and grain size with the intrinsic layer thickness, we have studied the microstructures of the nc-Si:H solar cells using Raman spectroscopy and X-ray diffraction (XRD) at the University of North Carolina at Chapel Hill, small angle X-ray scattering (SAXS) at Colorado School of Mines, and Atomic Force Microscopy (AFM) at NREL.

A 514.5-nm laser was used as an excitation source for obtaining the Raman scattering spectra. The measurements directly scanned on the nc-Si:H cells made on Ag/ZnO BR. The upper plot in Fig. 2 shows an example of the Raman spectra of nc-Si:H solar cells, where the curve can be decomposed into three components: a very sharp peak at 515-520 cm^{-1} from the crystalline phase, the middle term located at 490 cm^{-1} and assigned to grain boundaries or inter-medium order, and a broad peak at 480 cm^{-1} from the amorphous regions. A calculation using the intensity ratios of the three peaks gives an average of the crystalline volume fraction in the absorption depth probed by the excitation source. The lower plot in Fig. 2 shows the thickness dependence of the crystalline volume fraction for the cells made on Ag/ZnO BR. It clearly shows the increase of crystalline volume fraction from 60% to 80% when the thickness is increased from 0.3 μm to 2.0 μm.

The two sets of nc-Si:H solar cells were also characterized by XRD. As shown in Fig. 3, all three XRD peaks increase dramatically with the increase of thickness, but the (220) peak grows faster than the (111) and (311) peaks as illustrated by the top plot in Fig. 4. This demonstrates enhanced (220) preferred orientations with increasing thickness but shows this effect to be reduced on the BR substrate, consistent with the crystallite collisional growth mechanism. Analysis of the (220) linewidths yields increasing grain size with thickness, but the grain sizes are clearly smaller for the BR series compared to the SS series, suggesting grain collisions reduce grain size for a given film thickness. The lower plot of Fig. 4 shows that the XRD integrated intensity (sum of (111), (220), and (311) peaks) grows faster than a linear trend. This is consistent with increasing crystalline volume fraction with thickness. The larger integrated intensities for the SS series is likely due to the enhanced (220) preferred orientations shown in the upper plot of Fig. 4. Also, the nature of the substrate is known to play a role in the amorphous to microcrystalline transition [11].

Figure 5 shows the AFM images of two samples on SS substrate, one with a thickness of 0.3 μm and the other 2.0 μm. The images clearly show the increases in the size of the surface micro-features as well as the surface roughness. Similar results were observed on the samples deposited on Ag/ZnO, but with complex features due to the substrate texture. Figure 6 plots the

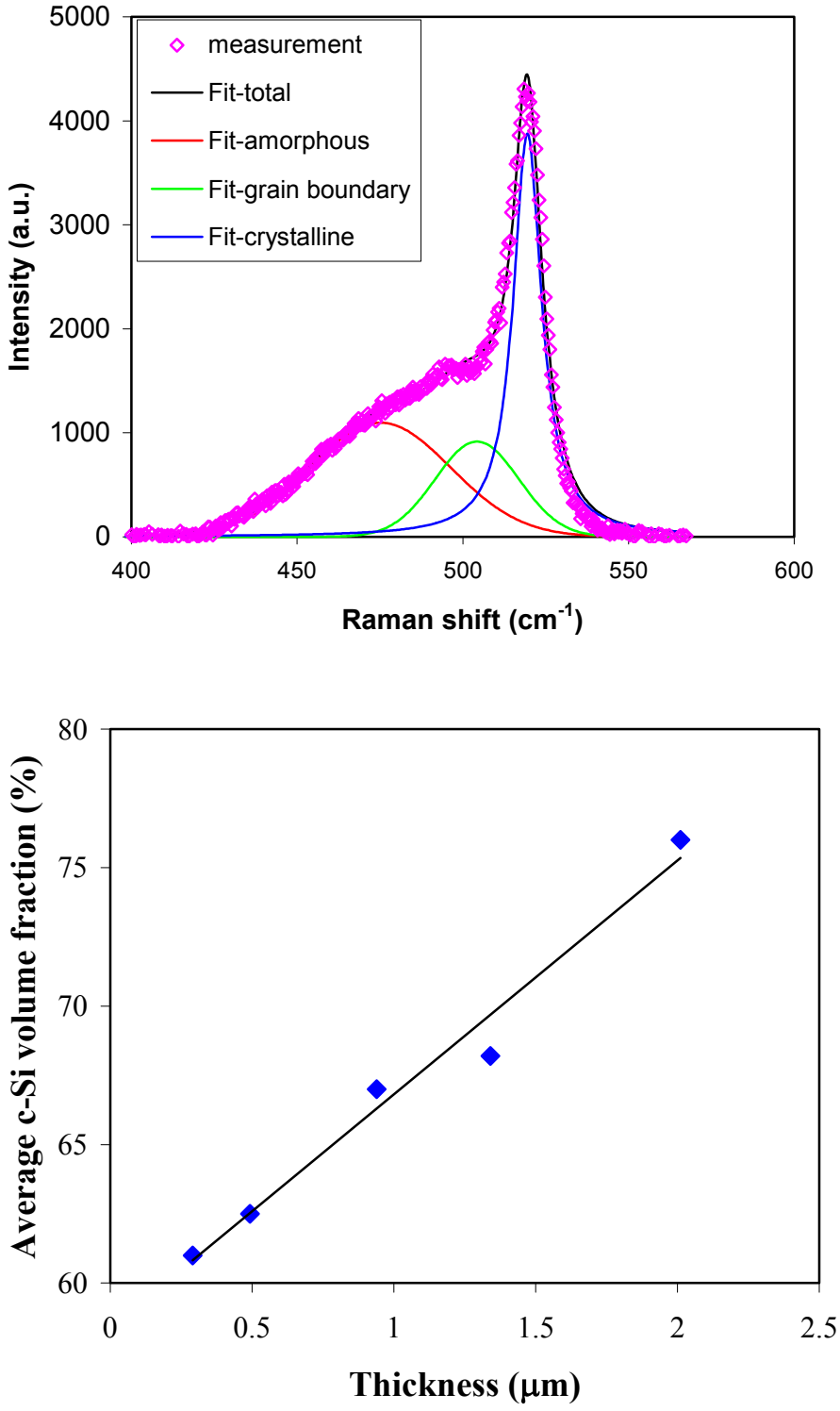

Figure 2. (upper) Raman spectrum of a nc-Si:H solar cell with three components of the decomposition and (lower) the average crystalline volume fraction versus cell thickness.

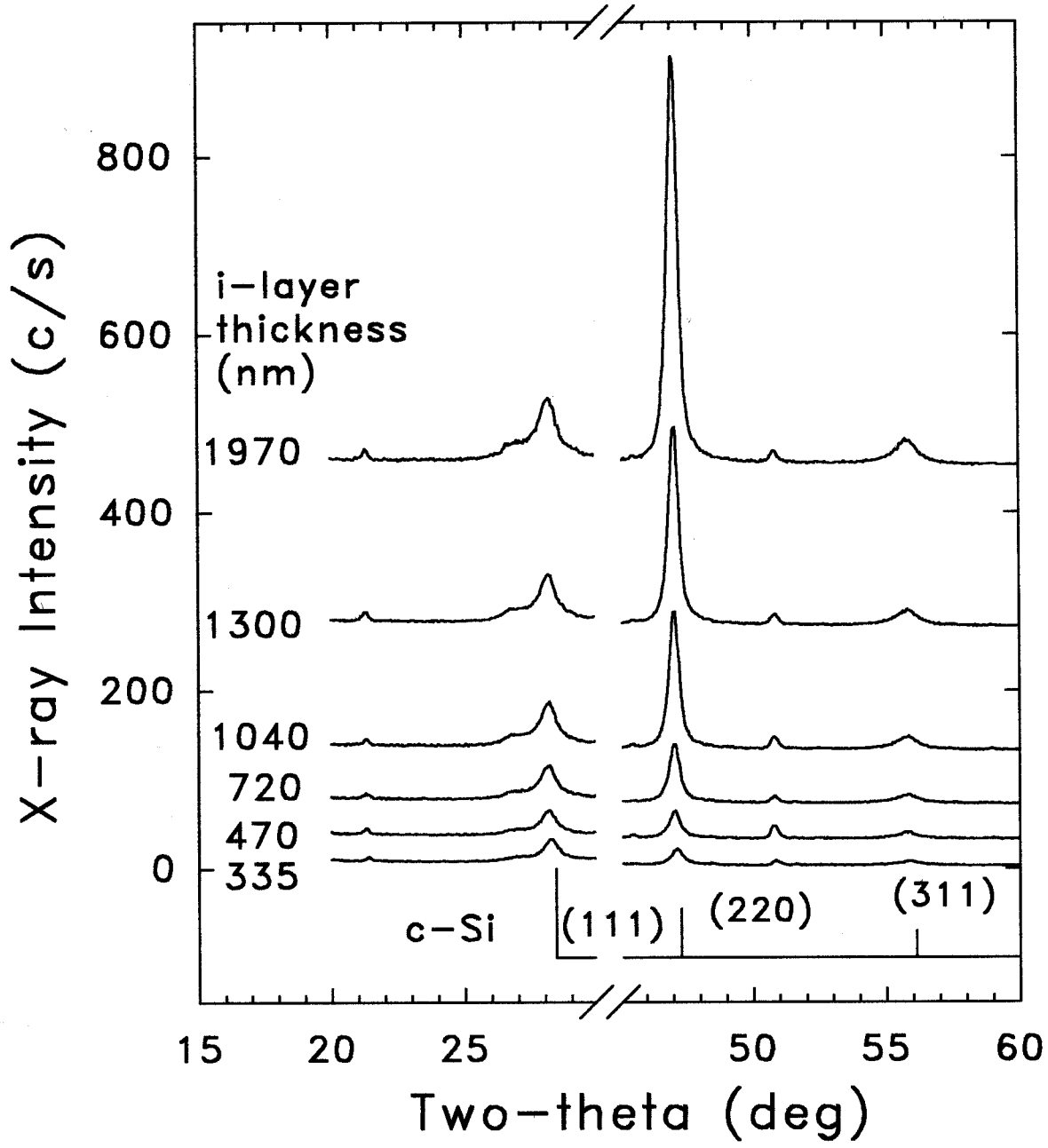

Figure 3. XRD patterns from the nc-Si:H solar cells on SS with different thicknesses. Stick diagram of c-Si random powder pattern is also shown.

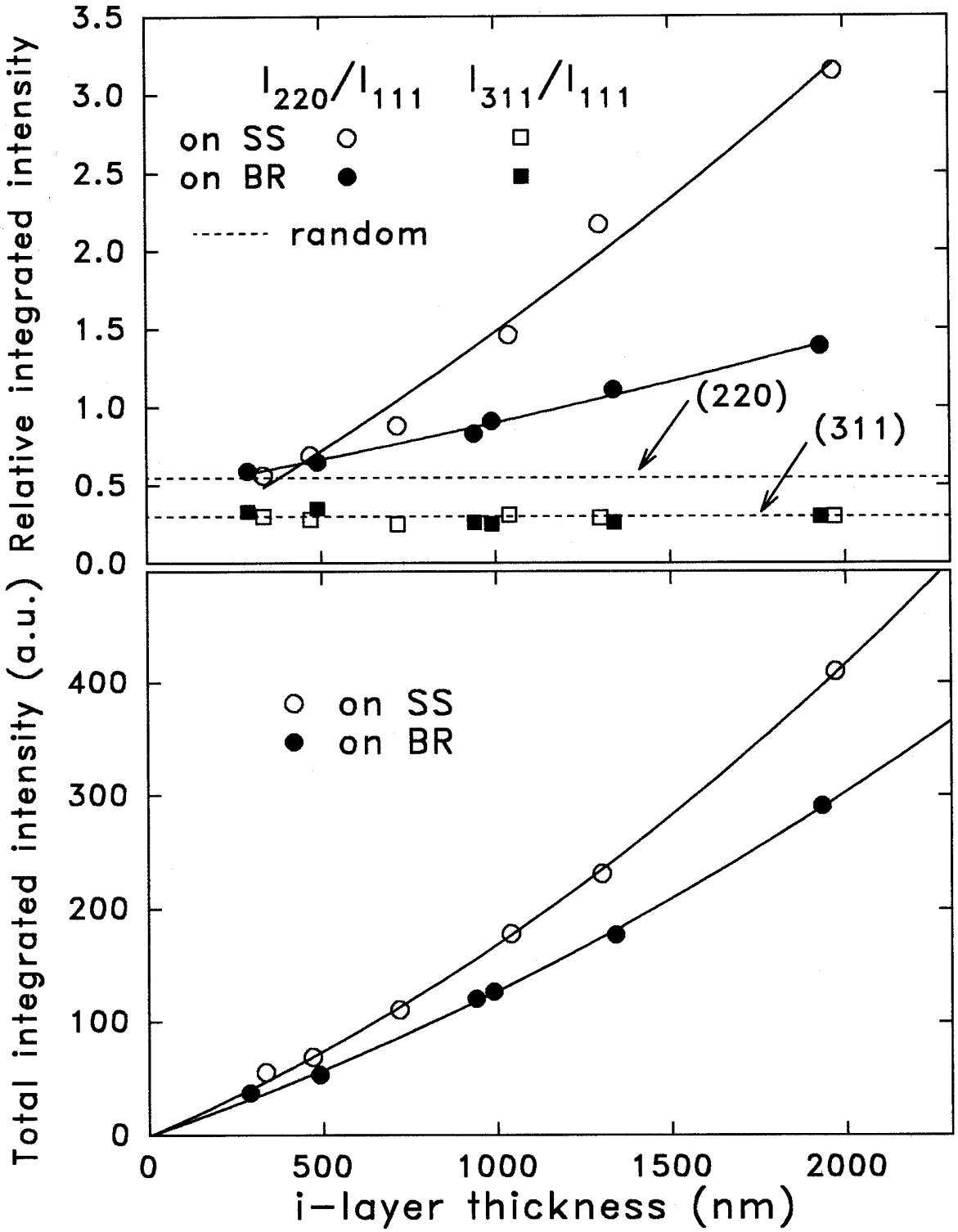

Figure 4. (upper) Relative and (lower) total integrated XRD intensities for the nc-Si:H solar cells. Solid lines were drawn to guide the eye.

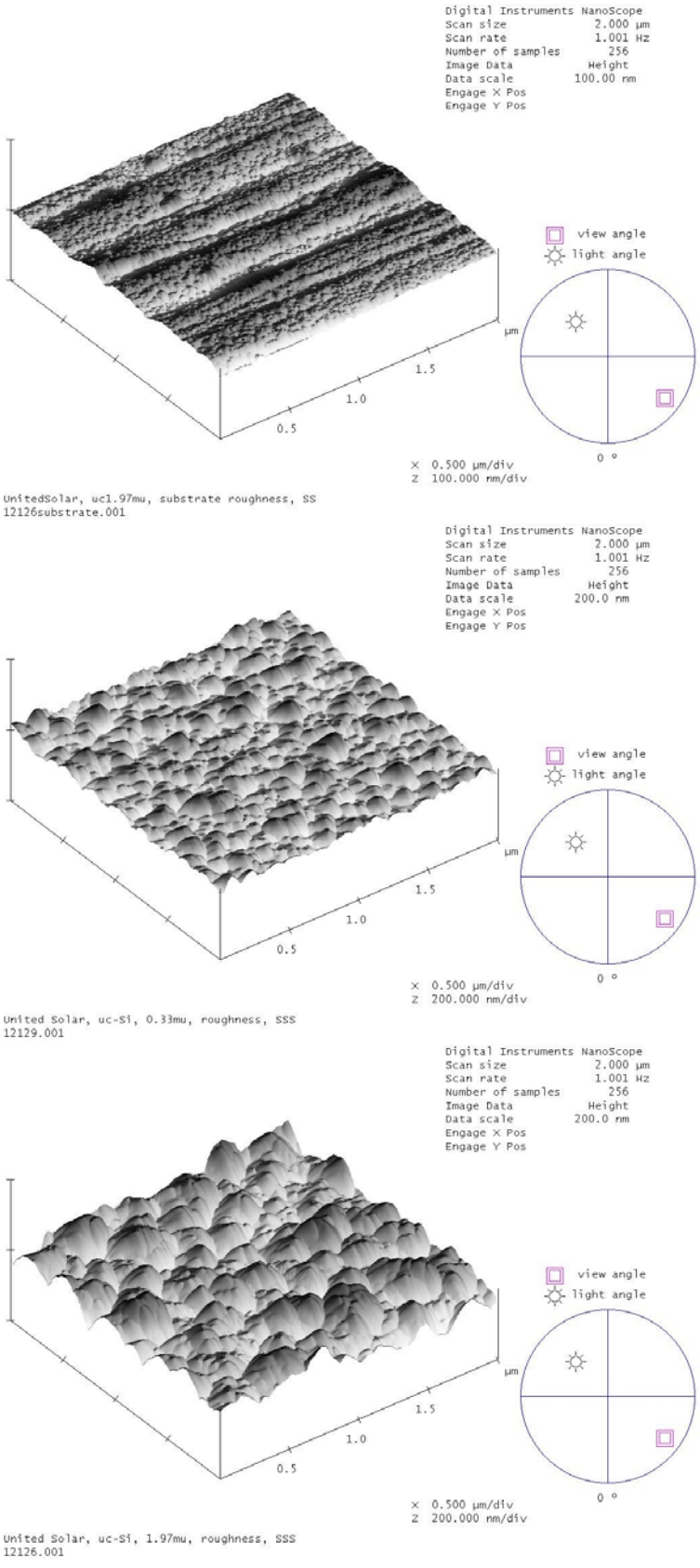

Figure 5. AFM images of (upper) a SS substrate, (middle) a 0.3 µm thick nc-Si:H solar cell and (bottom) a 2 µm thick nc-Si:H solar cell on SS substrate.

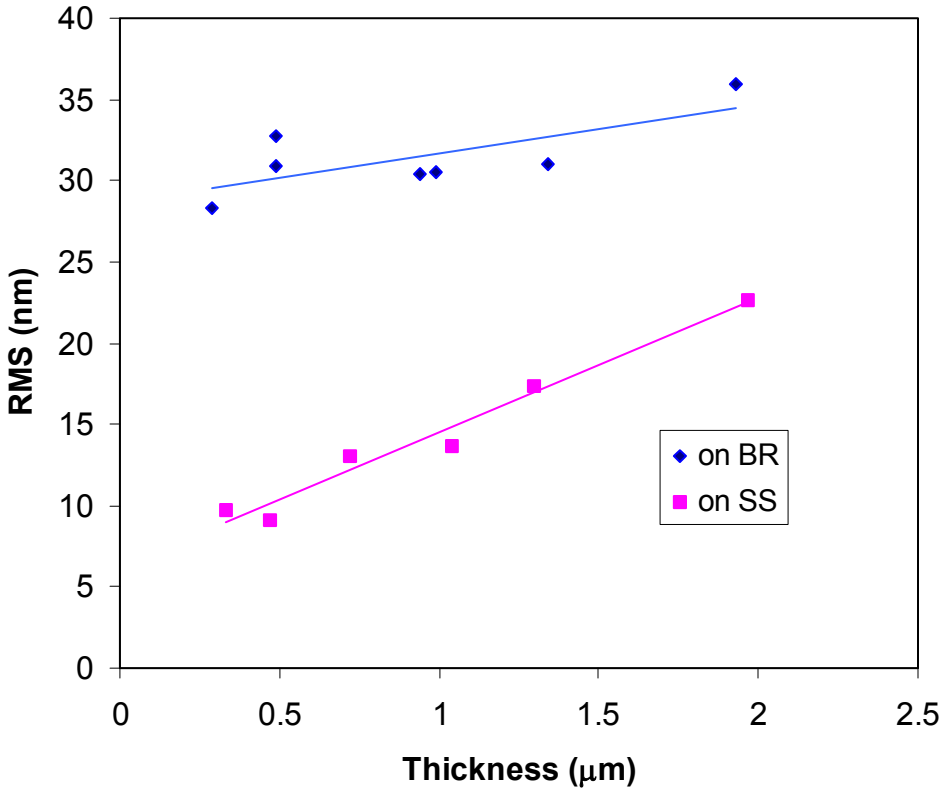

Figure 6. The surface roughness of the nc-Si:H solar cells versus the intrinsic layer thickness.

surface roughness defined as the root mean square (RMS) versus the cell thickness of the samples on BR and SS substrates. For the samples on SS, the roughness monotonically increases with increasing thickness, which is likely related to the evolution of the nanocrystallites in the nc-Si:H. However, for the cells on BR, the roughness also increases with thickness, but the total roughness is dominated by the surface of the substrate.

In summary, we have investigated the effect of the substrate and thickness on nc-Si:H solar cell performance. We found that the BR substrate has certain influence on cell performance and material structure, but it is not the main reason to cause the low J_{sc} of thick nc-Si:H solar cells at current stage. Therefore, we believe the increasing volume fraction of nc-Si:H with increasing thickness should be responsible for the low J_{sc} problem in thick nc-Si:H solar cell. The material analyses using Raman, XRD and AFM confirm that the crystalline volume fraction and grain size increase with the intrinsic layer thickness significantly.

2.4. Hydrogen Dilution Profiling in nc-Si:H solar cell deposition

From the results of thickness dependence of the cell performance and structure, we conjecture that the increase in crystalline volume fraction and grain size with intrinsic layer thickness is the main cause for the poor cell performance for thick nc-Si:H solar cells. The exact mechanism for such phenomenon is not clear. As suspected by Finger *et al*. [7], the poor grain boundary passivation could be the main problem for nc-Si:H material with high crystalline volume fraction and large grains. Of course, finding a way to obtain improved grain boundary passivation is a desirable approach for high efficiency nc-Si:H solar cell, especially for high crystalline volume fraction and large grain size. In the shorter term, we need to develop a way to avoid the increase of crystalline volume fraction and grain size and hence reduce the grain boundary defect density. It has been confirmed in many ways that the crystalline volume fraction and grain size grow with the nc-Si:H layer thickness when a constant hydrogen dilution ratio is used. Therefore, we believe that using a proper hydrogen dilution profile with reducing the hydrogen dilution ratio during the deposition to control the crystalline size and volume fraction could have some effect on the improvement of thick nc-Si:H cell performance.

The hydrogen dilution profiling technique has been used in the deposition of nc-Si:H solar cells using RF at a low rate ~ 1 Å/s and MVHF and a high rate 3-10 Å/s. Here we present the results of the nc-Si:H solar cells deposited using the LINE system with RF excitation at a low deposition rate ~ 1 Å/s. Textured Ag/ZnO BR was used as a substrate to enhance the light trapping effect. Table IV gives a summary of the J-V characteristics of nc-Si:H single-junction solar cells made with various hydrogen dilution profiles during the intrinsic layer deposition. The first five cells were made using the same recipe to check the reproducibility. It shows clearly that the fill factor (FF) has a large variation from run to run. A major factor that affects the reproducibility is the series resistance of the ITO. The ITO process was optimized for a-Si:H based solar cells, which have larger open-circuit voltage (V_{oc}), but lower J_{sc} than nc-Si:H solar cell. From the table, one can easily see that the cells with higher FF have lower series resistance. The series resistances listed in the table were deduced from the inverse of the derivative of the light J-V characteristics under the open circuit condition, which includes the contribution from the ITO resistance, junctions, and the intrinsic layer. At this moment, we are not sure whether the main portion of the series resistance is from the ITO or from the intrinsic layer. Although the baseline data are somewhat scattered, the average efficiency is around 6.6%, which is the maximum average value made in a thickness series for cells with the given dilution ratio.

Table IV. Summary of J-V characteristics of nc-Si:H single-junction solar cells made with various hydrogen dilution profiles. From Profiling 1 to Profiling 6, the slope of hydrogen dilution ratio versus time was increased.

Sample #	Eff (%)	J_{sc} (mA/cm^2)	V_{oc} (V)	FF			R_s ($\Omega.cm^2$)	Comments
				AM1.5	Blue	Red		
14554	6.74	22.58	0.495	0.603	0.652	0.615	4.4	Baseline
14568	6.48	22.15	0.488	0.599	0.648	0.599	4.0	
14592	6.78	21.32	0.488	0.642	0.690	0.658	3.1	
14594	6.61	20.79	0.486	0.654	0.687	0.648	3.1	
14596	6.61	22.05	0.482	0.622	0.656	0.605	4.0	
14559	6.54	21.48	0.482	0.632	0.678	0.637	4.0	20% thicker
14562	6.81	21.57	0.484	0.652	0.692	0.651	3.4	than baseline
14578	6.63	23.22	0.482	0.594	0.646	0.631	4.3	Profiling 1
14580	7.04	22.58	0.484	0.644	0.688	0.662	3.2	Profiling 2
14612	7.29	24.41	0.485	0.616	0.659	0.647	3.6	Profiling 3
14619	7.81	24.63	0.492	0.645	0.683	0.641	3.4	Profiling 4
14642	8.01	23.42	0.502	0.681	0.706	0.700	2.7	Profiling 5
14660	8.37	25.15	0.502	0.663	0.679	0.693	3.1	Profiling 6

Increasing the intrinsic layer deposition time by 20% did not increase the value of $J_{sc.}$ Instead, the response in the middle and long wavelength region was reduced. This phenomenon has been observed many times before. As shown in the previous sections, the increase of crystalline volume fraction and grain size with thickness is the main origin of the reduction of response in the middle and long wavelength regions. Proper hydrogen dilution profiling can control the crystalline growth evolution. We used this technique of reducing the hydrogen dilution ratio in the line machine during the intrinsic layer deposition to control the microstructure evolution. From Line Sample 14578 to 14660, we gradually increase the slope of the hydrogen dilution versus time. As a result, the cell performance has improved significantly. The J_{sc} has improved from approximately 22 mA/cm^2 in the baseline cells to over 25 mA/cm^2 in the best cell (Line 14660). The previous record for a nc-Si:H single-junction cell without hydrogen dilution profiling was an initial active-area efficiency of 7.4%. Using the hydrogen profiling technique, we achieved a new record of 8.4%. From Fig. 7, one can see that the middle and long wavelength responses have been significantly improved in the cell with proper hydrogen dilution profiling. Figure 8 plots the (a) J-V characteristics and (b) quantum efficiency of the best nc-Si:H single-junction solar cell.

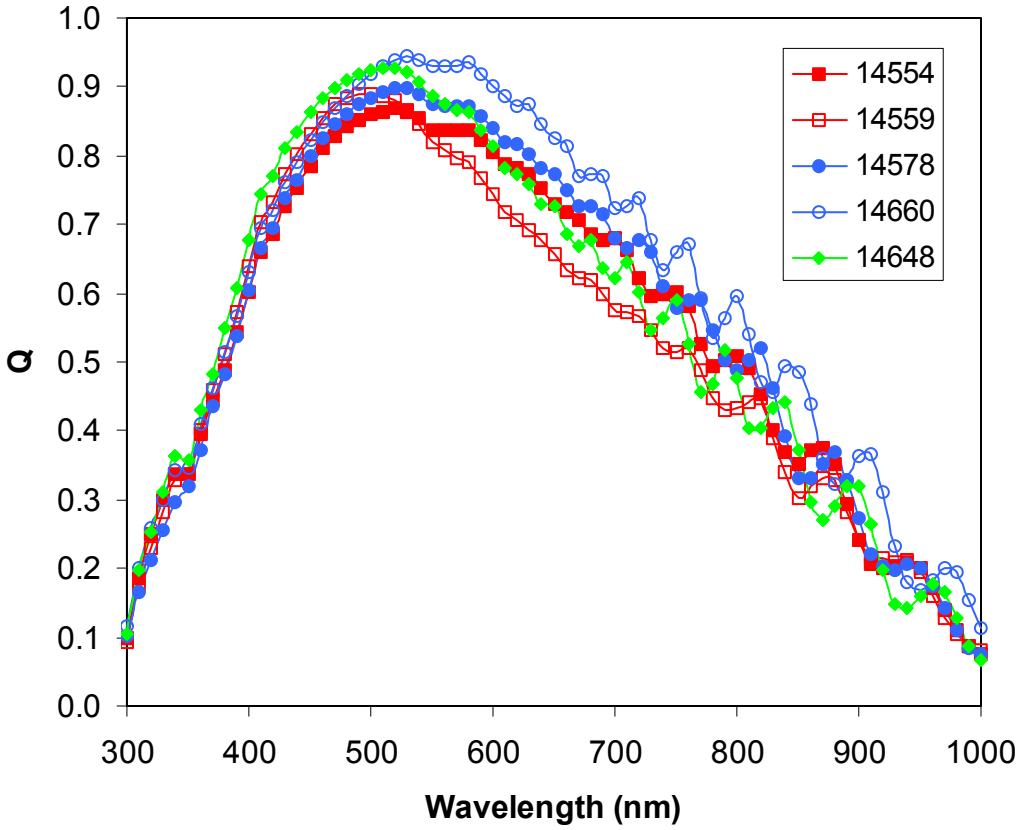

Figure 7. Quantum efficiency of nc-Si:H single-junction cells with various hydrogen dilution profiles. The sample number and the corresponding hydrogen dilution profiles are listed in Table IV.

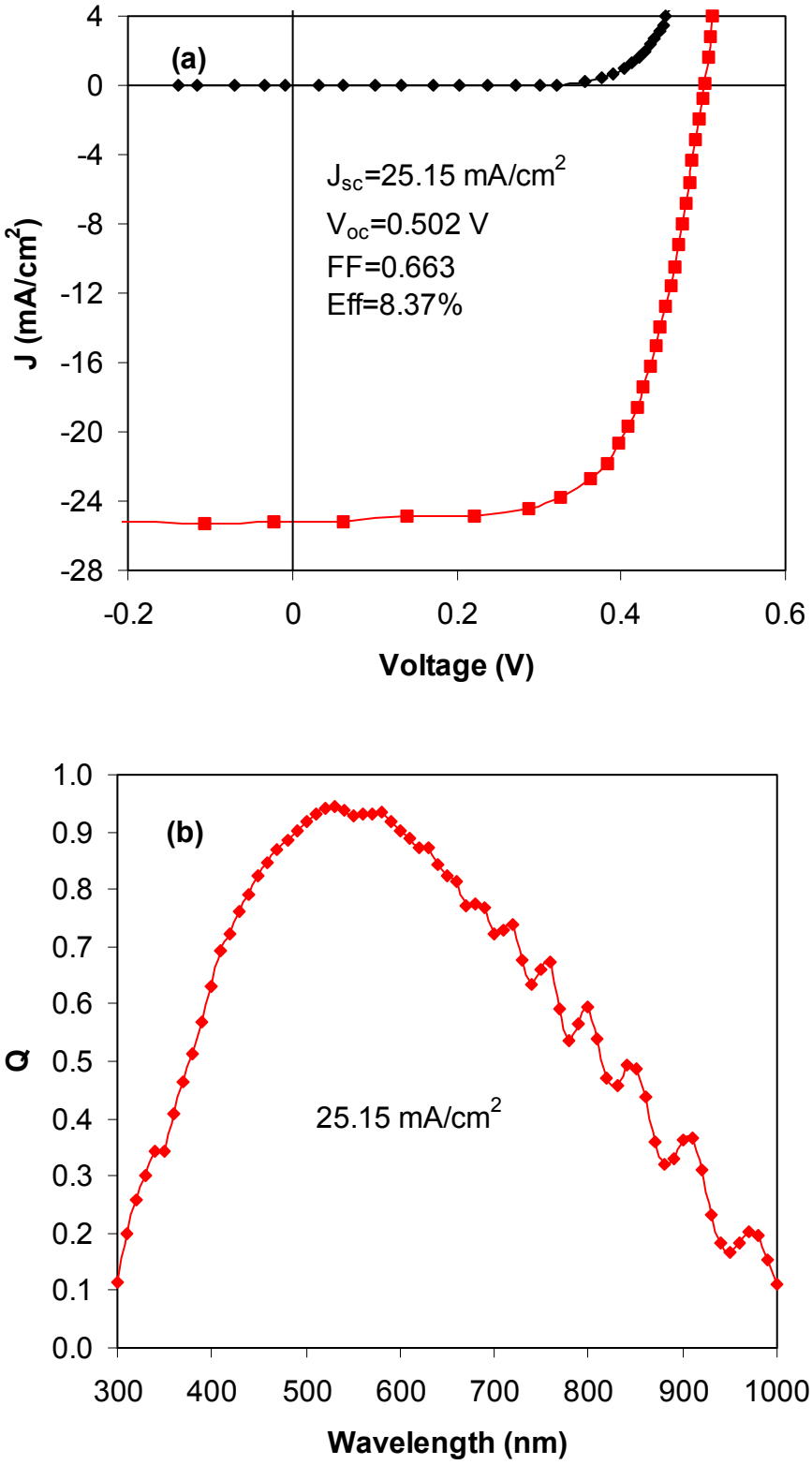

Figure 8. (a) J-V characteristics and (b) quantum efficiency of a nc-Si:H single-junction solar cell with an initial active-area efficiency of 8.37%.

Section 3: High Efficiency Multi-junction Cell with nc-Si:H Bottom Cell

3.1. Optimization of multi-junction solar cells

We have used the improved nc-Si:H cell in the a-Si:H/nc-Si:H double-junction and a-Si:H/a-SiGe/nc-Si:H triple-junction structures. We have achieved new record initial active-area efficiencies of 13.45% and 14.59% with the tandem and triple cell structures respectively. Figures 9 and 10 show the (a) J-V characteristics and (b) quantum efficiency of the best a-Si:H/nc-Si:H double-junction and a-Si:H/a-SiGe:H/nc-Si:H triple-junction solar cells, respectively. The 14.59% initial efficiency is close to the champion a-Si:H/a-SiGe:H/a-SiGe:H triple-junction cell [12] and the record a-Si:H/nc-Si:H double-junction cell reported by Kaneka Corp. [1].

Comparing the nc-Si:H single-junction cell to the a-Si:H/nc-Si:H double-junction and a-Si:H/a-SiGe:H/nc-Si:H triple-junction cells, we find that the FF of the multi-junction cell is much better than the nc-Si:H single-junction cell, especially for a bottom cell limited current mismatch. As shown in previous reports [3], the FF of a-Si:H/nc-Si:H double-junction cells under blue light illumination is as large as 0.83, indicating a high FF from the nc-Si:H bottom cell. However, we could hardly obtain a FF over 0.7 for nc-Si:H single-junction cells. The real reason for the difference in FF between the nc-Si:H single-junction cell and the a-Si:H/nc-Si:H double-junction cell is an interesting topic for us. In addition to the influence of series resistance from the ITO, we suspect that during the ITO processing, the nc-Si:H intrinsic layer gets degraded in the single-junction cell. SAXS measurements have shown that nc-Si:H has more microvoids than a-Si:H [13]. The ITO is evaporated in an oxygen-rich environment. Therefore, oxygen may have a large chance to diffuse into the nc-Si:H layer. In addition, the tolerance for impurity is lower for nc-Si:H cells than for a-Si:H cells. An alternate possibility is that because the nc-Si:H cell is generating a much lower current as a bottom cell and thus experiences a smaller Fermi level splitting compared to when it is functioning as a single cell, the FF value is higher in the former case.

3.2. Stability of a-Si:H/nc-Si:H double-junction and a-Si:H/a-SiGe:H/nc-Si:H triple-junction solar cells

One a-Si:H/nc-Si:H double-junction cell and one a-Si:H/a-SiGe:H/nc-Si:H triple-junction solar cell with similar initial efficiencies were light soaked under 100 mW/cm^2 of white light at 50 °C for over 1000 hours. Table V summarizes their initial and stable performance. The cells both stabilized at 11.8%. In this case, the triple-junction cell did not show an advantage over the double-junction cell. In fact, it degraded more. The high degradation in this a-Si:H/a-SiGe:H/nc-Si:H triple-junction cell is attributed to the middle-cell-limited current mismatching as shown in Table V. We know that the a-SiGe:H middle cell degrades more than the a-Si:H top cell and the nc-Si:H bottom cell. Although the thin a-Si:H top cell in the triple-junction cell might degrade less than the thick a-Si:H top cell in the double-junction-cell, the degradation in the a-SiGe:H middle cell results in a large total degradation in this triple-junction cell. In order to obtain a high stable efficiency, a bottom cell limited current mismatching is desirable. Currently, we are light soaking the champion a-Si:H/a-SiGe/nc-Si:H triple-junction cell shown in

Fig. 10, in which the a-SiGe:H middle cell has much higher current than the a-Si:H top cell and nc-Si:H bottom cell. We expect a high stable efficiency.

Table V. Summary of stability results of an a-Si:H/nc-Si:H double-junction solar cell (L14643) and an a-Si:H/a-SiGe:H/nc-Si:H triple-junction solar cell (L14682). The data in bold are the limiting J_{sc}.

Run #	state	Eff (%)	J_{sc} (mA/cm^2)			V_{oc} (V)	FF
			top	middle	bottom		
L14643	initial	13.45	12.75	—	**12.61**	1.439	0.741
	stable	11.81	**12.22**	—	12.38	1.399	0.691
	degradation	12.2%	4.2%		1.8%	2.8%	6.7%
L14682	initial	13.62	8.65	**8.14**	8.34	2.190	0.764
	stable	11.77	8.33	**7.82**	8.15	2.154	0.699
	degradation	13.6%	3.7%	3.9%	2.3%	1.7%	8.5%

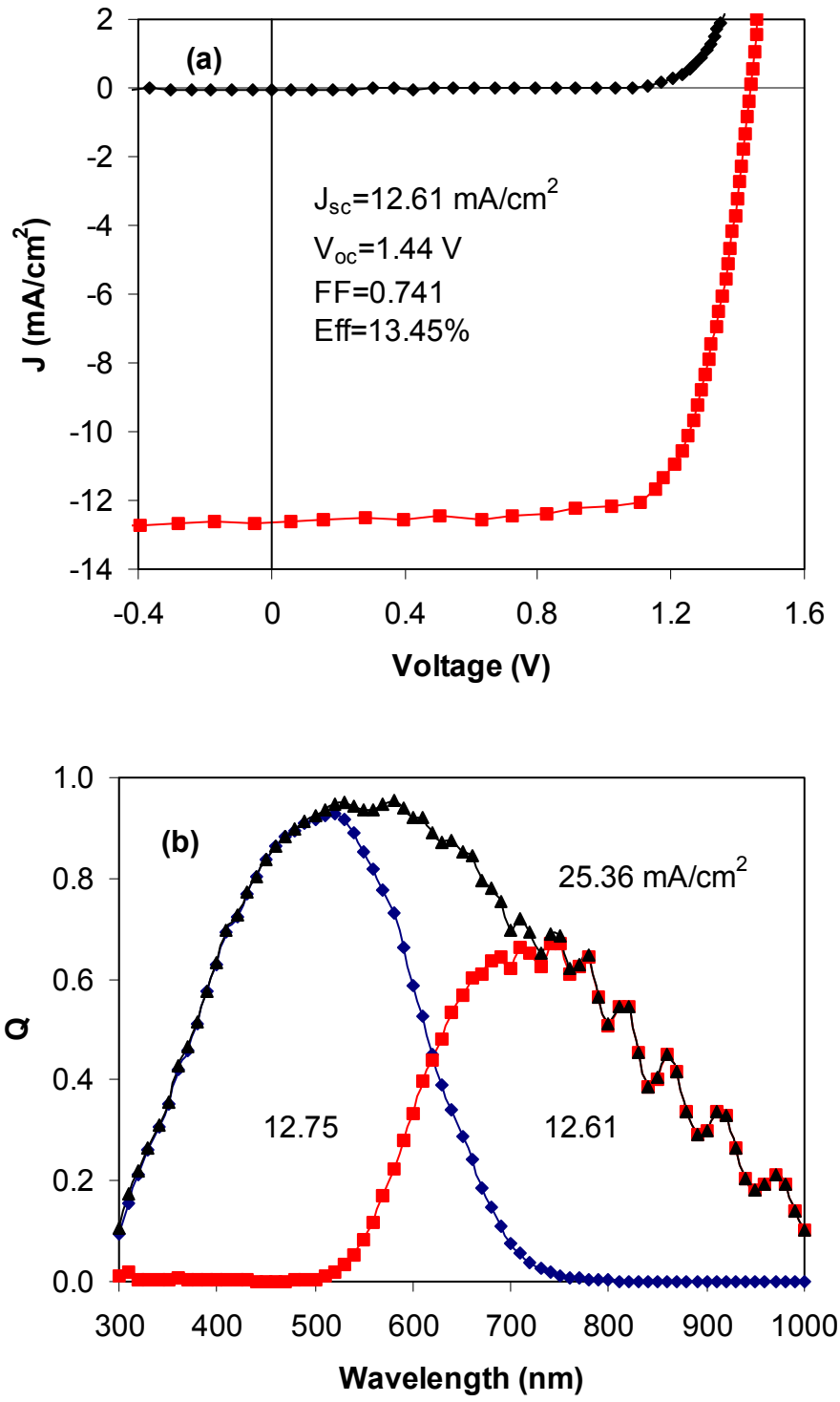

Figure 9. (a) J-V characteristics and (b) quantum efficiency of an a-Si:H/nc-Si:H double-junction solar cell with an initial active-area efficiency of 13.45%.

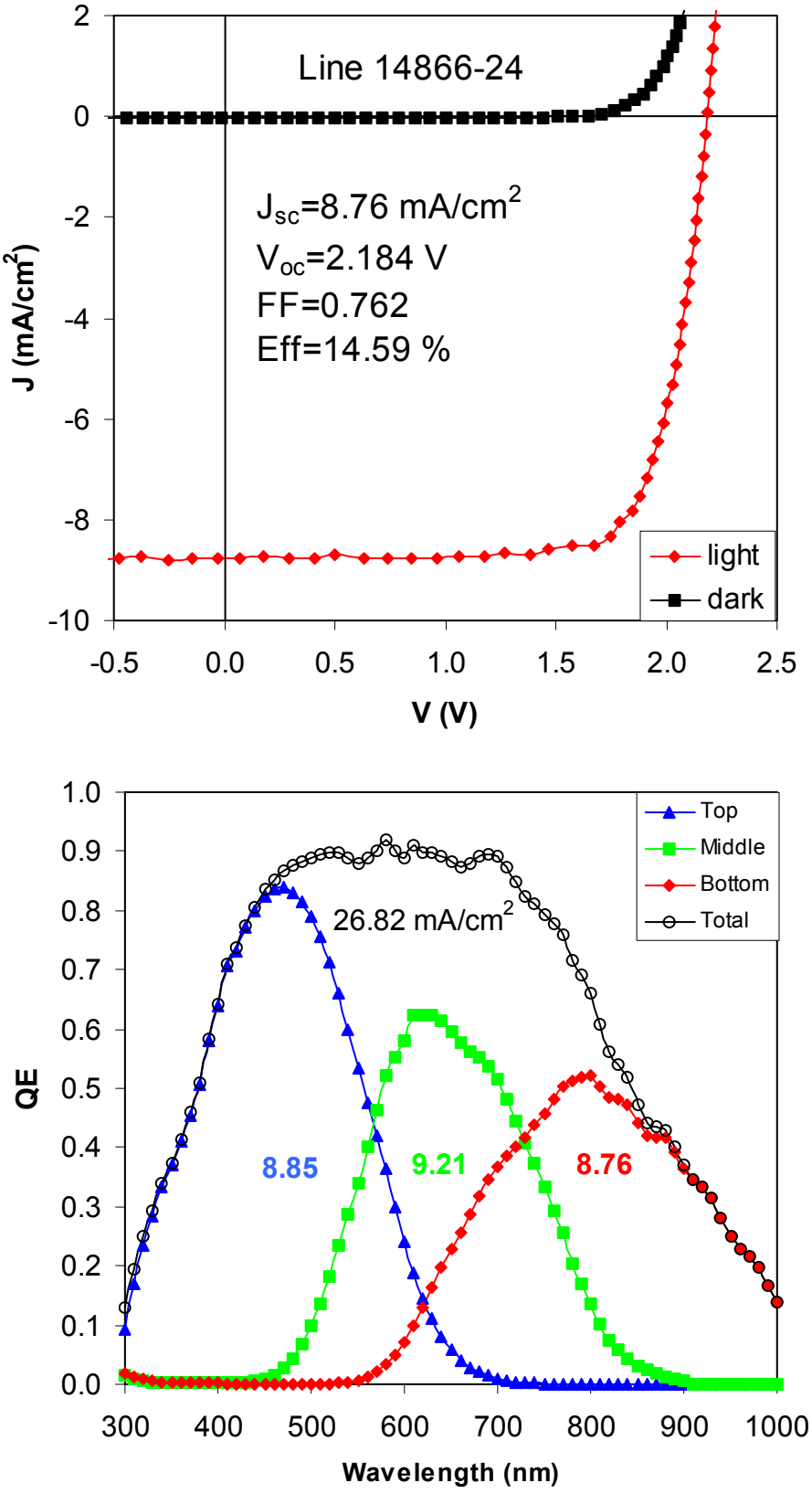

Figure 10. (a) J-V characteristics and (b) quantum efficiency of an a-Si:H/a-SiGe:H/nc-Si:H triple-junction solar cell made using RF glow discharge at a low rate ~1 Å/s.

Section 4: High Rate Deposition of nc-Si:H Single-junction and Multi-junction Solar Cells Using Modified VHF Glow Discharge

In previous reports, MVHF has been shown to be a powerful technique for high quality nc-Si:H deposition at high rates. With this technique, we have achieved initial active-area efficiencies of 7.1% in a nc-Si:H single junction solar cell and 12.5% in an a-Si:H/nc-Si:H double-junction structure. In this fiscal year, the work continues to be focused on optimizing the recipe of nc-Si:H growth. In conjunction, we started to make triple-junction cell with a structure of a-Si:H/a-SiGe:H/nc-Si:H in order to pursue the higher initial and stabilized efficiencies in multi-junction solar cells. A new efficiency record of 7.7% has been achieved in a single junction cell. Moreover, we obtained a 12.8% initial efficiency in an a-Si:H/a-SiGe:H/nc-Si:H triple-junction cell with a bottom cell deposition time of 60 minutes. By taking advantage of a lower degradation in nc-Si:H than a-Si:H and a-SiGe:H alloys, we have minimized the light induced degradation in triple junction structures by designing a bottom-cell-limited current mismatching, and obtained a stable active-area cell efficiency of 11.4%.

4.1. Experimental

A multi-chamber system with three RF chambers and one MVHF chamber is used to deposit nc-Si:H single and multi-junction solar cells. The *nip* structures were deposited on Ag/ZnO back reflector (BR) coated stainless steel (SS) substrates. The a-Si:H and nc-Si:H intrinsic layers were prepared using the MVHF glow discharge with an excitation frequency of 65-75 MHz. The doped and buffer layers were deposited with RF glow discharge as was the a-SiGe:H intrinsic layer of the middle cell in the a-Si:H/a-SiGe:H/nc-Si:H triple-junction devices. The solar cells were completed with indium-tin-oxide dots having an active-area of 0.25 cm^2 on the top *p* layer. Current density versus voltage, J-V, characteristics were measured under an AM1.5 solar simulator at 25 ^oC. Quantum efficiency (Q) was measured from 300 to 1000 nm. Stabilized efficiencies were obtained by > 1000 hours light soaking under a 100 mW/cm^2 white light at 50 ^oC.

4.2. MVHF high rate nc-Si:H single-junction solar cell

For obtaining high efficiency multi-junction solar cells, a prerequisite is to develop a high quality nc-Si:H material and solar cell. Previously, we have reported a nc-Si:H single-junction solar cell with an initial active-area efficiency of 7.1%, where the intrinsic layer was deposited in 50 minutes. The main limitations to obtaining higher efficiency are low J_{sc} and fill factor (FF). It is well known that FF critically depends on the microstructure of the material. A material containing a high density of microvoids or cracks normally has a high density of defects related to poor grain boundary passivation and contamination due to post oxygen diffusion [3]. We have found that the increase of grain size and microcrystalline volume fraction with increasing thickness is the main obstacle for obtaining high efficiency in thick nc-Si:H solar cells as discussed in Section 1. To solve this problem, we used the hydrogen dilution profiling technique to keep the nc-Si:H material structure close to the nanocrystalline/amorphous transition region throughout the entire intrinsic layer as discussed in the previous section. So far, we have not used the hydrogen dilution profiling technique in MVHF deposition. Instead, we use a relatively

thin nc-Si:H bottom cell. First, a thin nc-Si:H bottom cell can be deposited in a relatively short time, which is desirable from the cost-effective point of view; second, a thin nc-Si:H bottom cell is less susceptible to the enhanced nanocrystalline evolution, and therefore has better V_{oc} and FF than a thick one. Although J_{sc} is low for the thin nc-Si:H cells, it does not cause significant efficiency reduction in multi-junction cells at the present stage, especially when a strong bottom-cell-limited current mismatching is used. Based on this analysis, we have made thin nc-Si:H single-junction cells with the intrinsic layer thickness around 0.5 to 0.7 μm. The best nc-Si:H cell has an initial active-area efficiency of 7.7%. The J-V characteristics and quantum efficiency are shown in Fig. 11.

4.3. MVHF high rate a-Si:H/nc-Si:H double-junction and a-Si:H/a-SiGe:H/nc-Si:H triple-junction solar cells

By improving the nc-Si:H material quality and optimizing the device configuration, a 12.5% initial active-area efficiency has been achieved using an a-Si:H/nc-Si:H double-junction solar cell, which was shown in last annual report. In order to take full advantage of the high current capability of nc-Si:H in a-Si:H/nc-Si:H double junction solar cells, a thick a-Si:H top cell is needed to meet the current mismatching requirement. Such thick a-Si:H cells normally degrade more than a thin one, and thus the benefit of the nc-Si:H material is not fully realized. An internal reflection layer between the a-Si:H and nc-Si:H has been used to address the problem [1]. In our laboratory, we use an a-Si:H/a-SiGe:H/nc-Si:H triple-junction structure, where the a-Si:H top and a-SiGe:H middle cells are not very thick, thus no significant degradation is expected. As shown in Section 2, an initial active-area efficiency of 14.6% has been achieved using this triple-junction structure at a low rate ~ 1 Å/s. During the past year, we focused on the optimization of the a-Si:H/a-SiGe:H/nc-SiGe:H triple-junction cell using MVHF at high rates and achieved an initial active-area efficiency of 12.8% and a stable active-area efficiency of 11.4%. Figure 12 shows the J-V characteristics and quantum efficiency curves of the initial and stable efficiency of this a-Si:H/a-SiGe:H/nc-Si:H triple-junction solar cell. The deposition time of the bottom cell intrinsic layer in this triple-junction cell was 60 minutes. The cell has a bottom cell limited current and a high FF of 0.791, indicative of a high quality nc-Si:H material.

4.4. Stability of the high rate multi-junction solar cells with nc-Si:H bottom cell

Next, we address the stability issue of the high rate multi-junction solar cells with a nc-Si:H bottom cell. First, we present the light soaking result of the champion a-Si:H/nc-Si:H double-junction solar cell with an initial active-area efficiency of 12.5%. Figure 13 shows the (a) J-V characteristics and (b) quantum efficiency of this cell. After over 1000 hours of light soaking, the efficiency degraded to 11.0%, which is the highest stable efficiency for the a-Si:H/nc-Si:H double-junction solar cells made at high rates.

As known from our previous report, the light-induced degradation strongly depends on the current mismatching in a-Si:H/nc-Si:H double junction solar cells. The degradation could be 5% for a cell with a strong bottom cell limited current mismatching to 16% for a cell with a matched current or a top cell limited current mismatching. A similar experiment was done with a-Si:H/a-SiGe:H/nc-Si:H triple-junction solar cells. Table VI lists the initial and stabilized cell

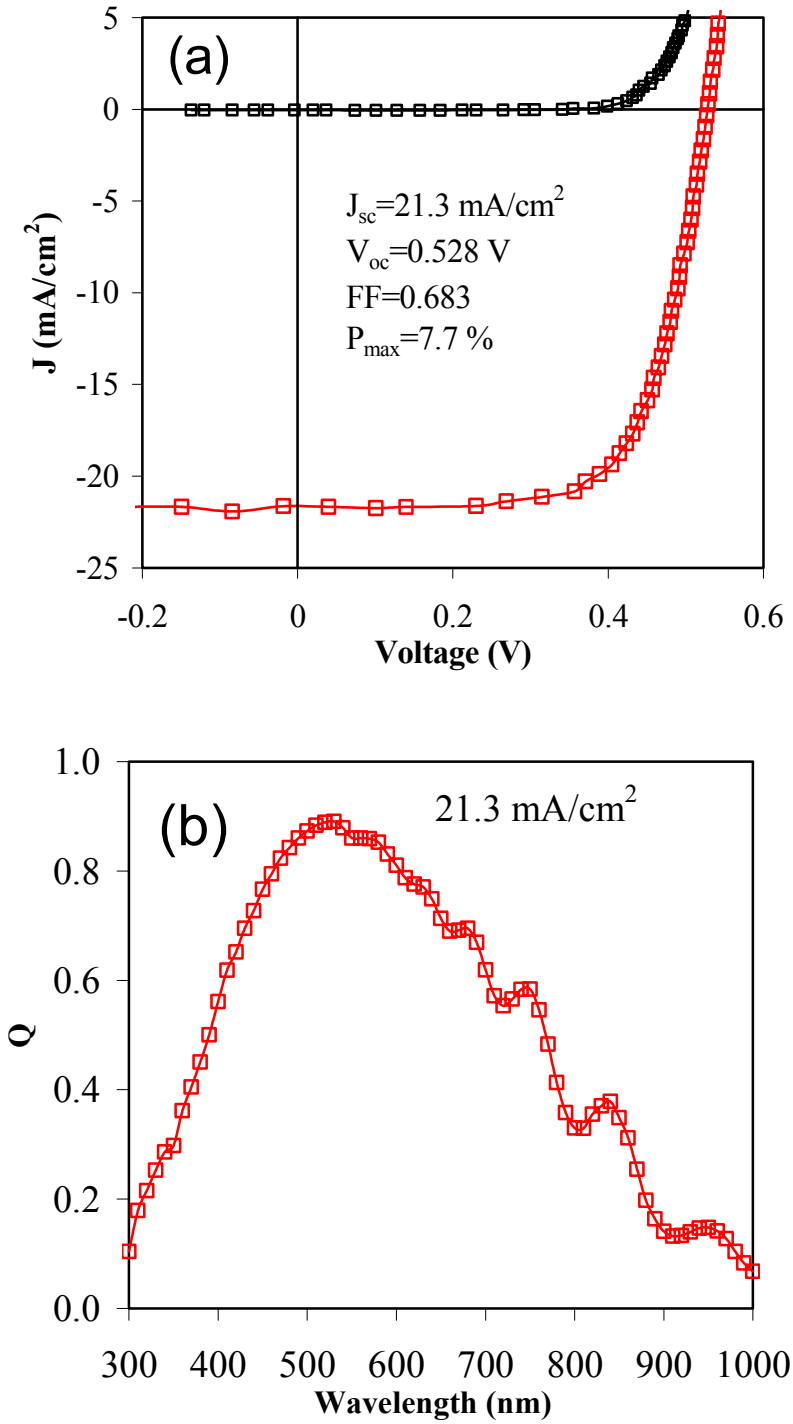

Figure 11. (a) J-V characteristics and (b) quantum efficiency of a νc-Si:H single junction solar cell with an intrinsic layer thickness of 0.6 μm.

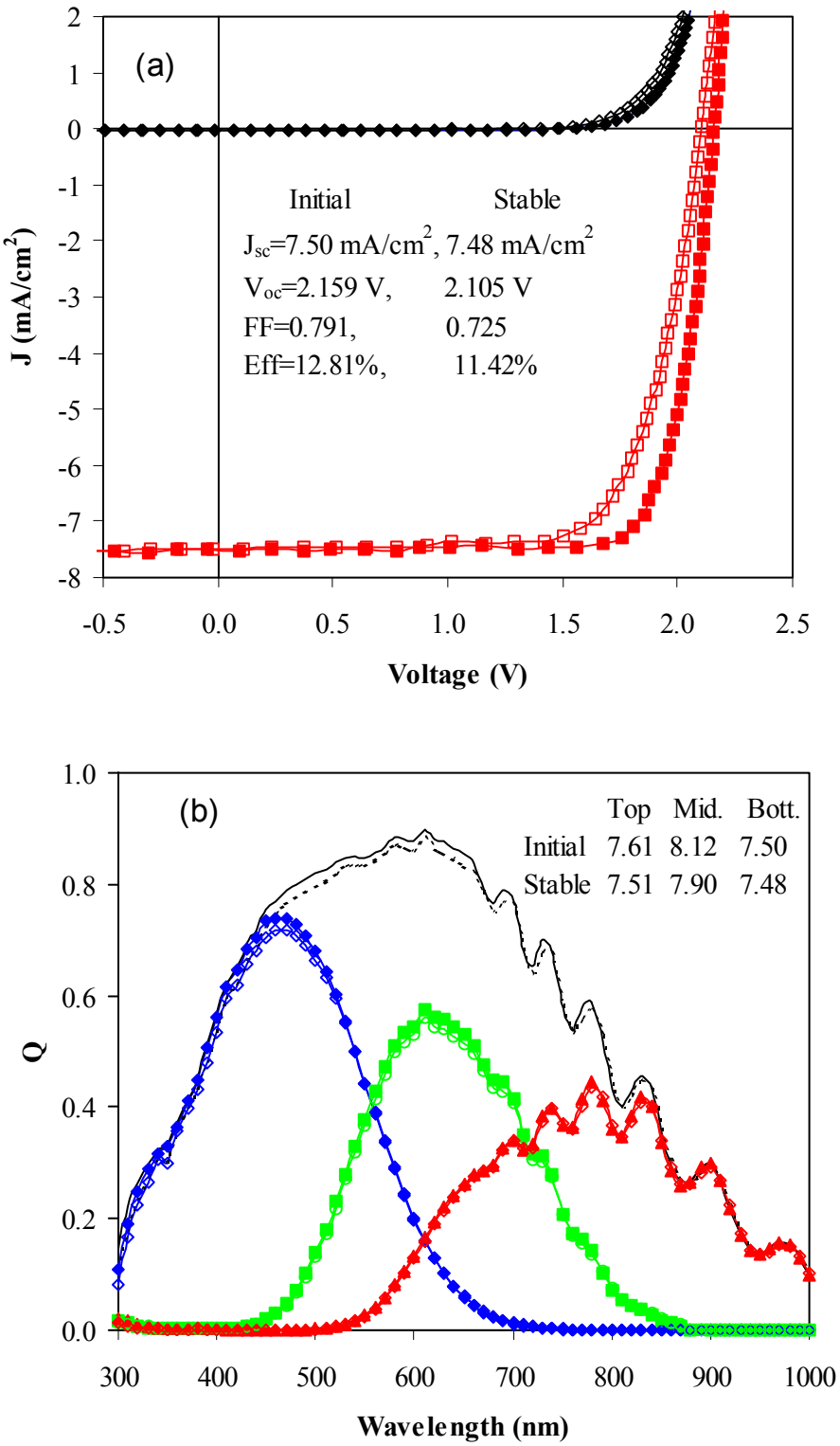

Figure 12. (a) Initial and stable J-V characteristics, and (b) quantum efficiency in an a-Si:H/a-SiGe:H/nc-Si:H triple-junction solar cell.

performance for four cells with different current mismatching. One can see the cell (#12468) with a strong bottom cell limited current mismatching has the lowest light induced degradation. Clearly, it benefits from the bottom cell limited design. Overall, the a-Si:H/a-SiGe:H/nc-Si:H triple-junction cells show a degradation in the range from 8 to 15%, which is similar to the degradation in a-Si:H/nc-Si:H double-junction solar cells. The highest active-area stable efficiency for the a-Si:H/a-SiGe:H/nc-Si:H triple-junction cell is 11.4%, which is from the cell with the highest initial active area efficiency of 12.8% as shown in Fig. 12. Although the top cell is thinner in the triple-junction structure, the degradation in the less stable a-SiGe:H middle cell has affected the overall degradation.

4.5. Summary

We have made nc-Si:H single-junction solar cells using MVHF at high deposition rates and achieved an initial active-area efficiency of 7.7%. We used the improved nc-Si:H cell as the bottom cell in multi-junction structures. Initial active-area efficiencies of 12.5% and 12.8% have been achieved using a-Si:H/nc-Si:H double-junction and a-Si:H/a-SiGe:H/nc-Si:H triple-junction structure, respectively. We conducted light soaking experiments on both the double-junction and triple-junction structures and found that the light induced degradation is in the range from 8 to 15%, depending on the material quality and the cell current mismatching. Similar to the a-Si:H/nc-Si:H double-junction structure, a bottom-cell-limited current mismatching results in low light-induced degradation in the a-Si:H/a-SiGe:H/nc-Si:H triple-junction structure. Stable efficiencies of 11.0% and 11.4% have been obtained using an a-Si:H/nc-Si:H double-junction and an a-Si:H/a-SiGe:H/nc-Si:H triple-junction structure, respectively.

Table VI. Initial and stable J-V characteristics of four a-Si:H/a-SiGe:H/nc-Si:H triple-junction solar cells. The numbers in bold are the limiting current densities. The highest stabilized efficiency is 11.4%.

Sample No.	State	V_{oc} (V)	FF	J_{sc} (mA/cm^2)	Q (mA/cm^2)			Eff (%)
					Top	Mid.	Bott.	
12427	Initial	2.203	0.730	7.42	8.19	**7.42**	7.68	11.93
	Stable	2.122	0.669	7.18	7.93	**7.18**	7.69	10.19
	Degr.	3.68%	8.36%	3.23%	3.17%	3.23%	0%	14.6%
12660	Initial	2.146	0.760	7.20	7.20	**8.22**	7.48	11.74
	Stable	2.092	0.679	7.06	7.06	**8.00**	7.53	10.03
	Degr.	2.52%	10.66%	1.94%	1.94%	2.68%	0%	14.6%
12468	Initial	2.165	0.790	7.16	7.56	7.95	**7.16**	12.25
	Stable	2.117	0.746	7.10	7.34	7.64	**7.10**	11.21
	Degr.	2.27%	5.57%	0.84%	2.91%	3.90%	0.84%	8.5%
12667	Initial	2.159	0.791	7.50	7.61	8.12	7.50	12.81
	Stable	2.105	0.725	7.48	7.51	7.90	7.48	11.42
	Degr.	2.50%	8.34%	0.26%	1.31%	2.71%	0.26%	10.9%

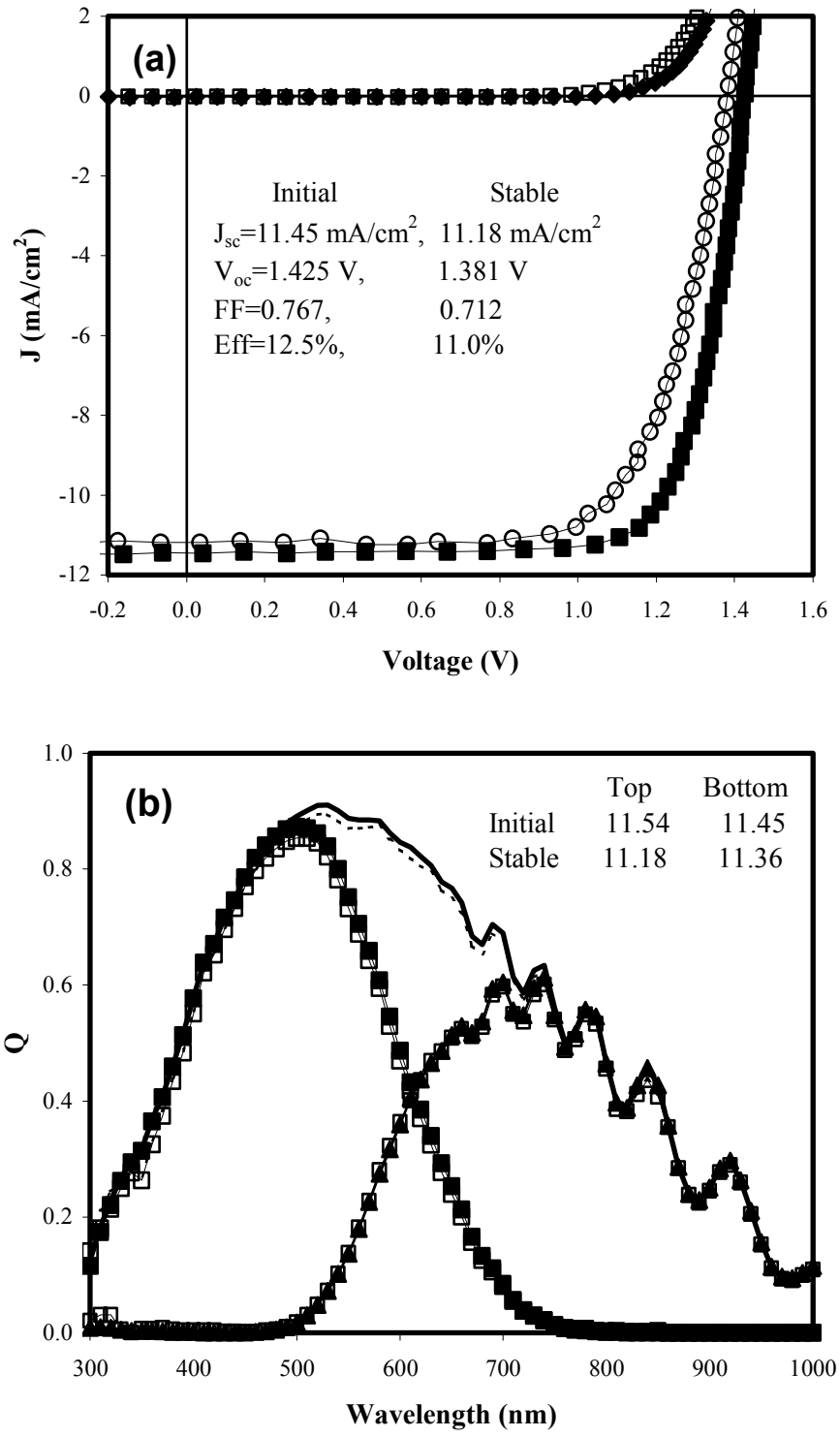

Figure 13. (a) Initial and stable J-V characteristics, and (b) quantum efficiency in an a-Si:H/nc-Si:H double junction solar cell.

Section 5: High Rate Deposition of nc-Si:H Solar Cells Using RF Glow Discharge in the High Pressure Regime

As reported in the literature, successful methods for high rate deposition of nc-Si:H solar cells are VHF glow discharge [4] and RF glow discharge under high pressures with high power [6][14]. As an industrial R&D group, we need to evaluate both methods and study the feasibility of each method for the manufacturing process. We have made significant efforts in the deposition of nc-Si:H solar cell using MVHF and reasonable results have been obtained as presented in previous section and in the Phase I annual report. During this year, we started the study of high rate nc-Si:H deposition using RF glow discharge under high pressure with high power.

5.1. Experimental

A multi-chamber RF glow discharge has been used for nc-Si:H solar cell deposition. Single-junction nc-Si:H *n-i-p* cells were deposited on Ag/ZnO back reflector coated stainless steel substrate. The doped layers were deposited using the same optimized conditions as used for conventional a-Si:H/a-SiGe:H/a-SiGe:H triple-junction solar cells. We have searched in parameter space for the intrinsic nc-Si:H layer deposition conditions, including hydrogen dilution, substrate temperature, RF power and pressure. We found that higher hydrogen dilution is required to reach the transition from amorphous to microcrystalline under higher pressures. High substrate temperature helps to reduce the required hydrogen dilution, but our better solar cells were made at a relatively low temperature and with high hydrogen dilution.

5.2. RF high rate nc-Si:H single-junction cell

As expected, the high pressure RF glow discharge suffered from uniformity problems. The cell performance is not uniform even on a 2" × 2" substrate. Table VII lists the J-V characteristics of solar cells at different locations on the substrate. It appears that the cells in the center have high V_{oc} but low J_{sc}, indicating a low nanocrystalline volume fraction in the center. The highest efficiency for single-junction nc-Si:H is 6.7%, in which the intrinsic layer was deposited for 60 minutes. Figure 14 shows the J-V characteristics and quantum efficiencies of cells in the center and at the edge. From the quantum efficiency plot, one can see the long

Table VII. Initial active-area J-V characteristics of nc-Si:H single-junction cells made with RF under high pressure at high rate. The nc-Si:H deposition time was 60 minutes.

Sample #	Position	Eff (%)	J_{sc} (mA/cm^2)	V_{oc} (V)	$FF_{AM1.5}$	FF_{blue}	FF_{red}
7693	Center	6.6	21.44	0.517	0.598	0.662	0.670
	Edge	6.3	22.10	0.497	0.573	0.639	0.638
	Corner	5.6	23.60	0.468	0.509	0.604	0.601
7699	Center	6.7	22.48	0.494	0.605	0.651	0.604
	Edge	6.5	23.57	0.474	0.580	0.624	0.597

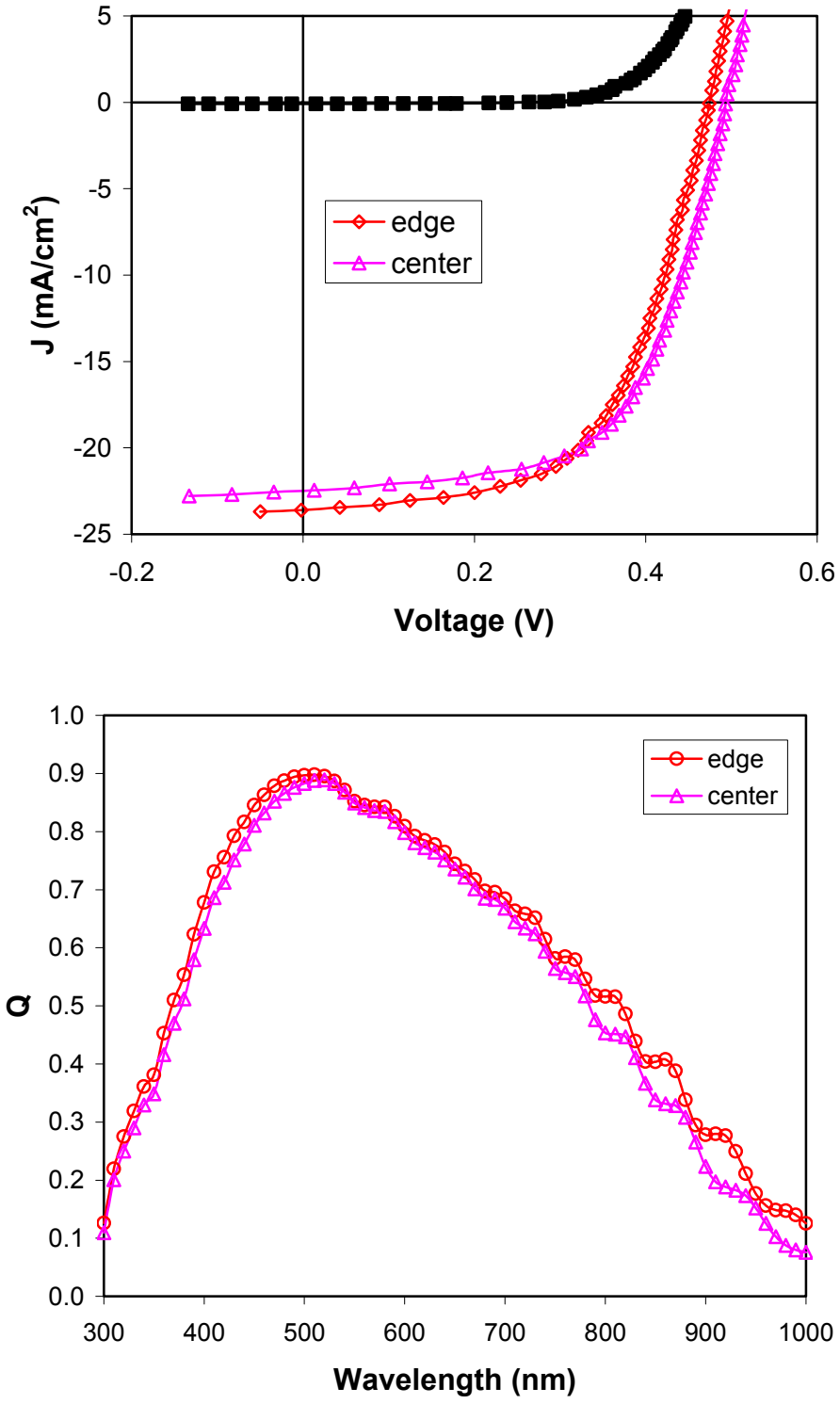

Figure 14. J-V characteristics and quantum efficiency of nc-Si:H single-junction cells at the center and the edge of the substrate. The nc-Si:H layer was deposited using high pressure RF glow discharge at ~ 3 Å/s for 60 minutes.

wavelength response is higher for the cell on the edge than in the center. The uniformity depends not only on the plasma parameters such as pressure, gas flow and RF power, but also on the reactor geometry such as the shape of the cathode and the gap between the cathode and the anode. Based on the properties of the high pressure RF plasma, we are currently working on further improvement of cell performance and uniformity. Another potential problem for the high-pressure deposition is powder formation, which affects the yield significantly. By optimizing the hardware design and deposition parameters, we have been able to avoid powder formation in the chamber after many runs under high-pressure deposition conditions.

5.3. RF high rate a-Si:H/nc-Si:H double-junction solar cell

We used the RF high rate nc-Si:H cell as the bottom cell in an a-Si:H/nc-Si:H double-junction structure and achieved an initial active-area efficiency of 12.3%, where the bottom cell nc-Si:H layer was deposited for 2 hours. Table VIII lists the J-V characteristics of three cells made with different bottom cell deposition times and Fig. 15 plots the J-V characteristics and quantum efficiency of the best a-Si:H/nc-Si:H double-junction cell.

5.4. Summary

We have started RF glow discharge deposition of nc-Si:H solar cells under a high pressure depleting regime with high power to achieve a high deposition rate. We achieved an initial active-area efficiency of 6.7% with a nc-Si:H single-junction cell and 12.3% with an a-Si:H/nc-Si:H double-junction cell. Currently we are working on the further optimization of cell efficiency and uniformity. We also need to increase the deposition rate further to reduce the deposition time.

Table VIII. Initial active-area J-V characteristics of a-Si:H/nc-Si:H double-junction cells made with RF glow discharge under high pressure at 3 Å/s. t is the nc-Si:H deposition time.

Sample #	t (min)	Eff (%)	J_{sc} (mA/cm^2)		V_{oc} (V)	FF
			Top	Bottom		
7727	60	10.0	12.38	9.60	1.439	0.722
7742	90	11.9	11.82	11.63	1.403	0.730
7741	120	12.3	11.89	12.69	1.410	0.731

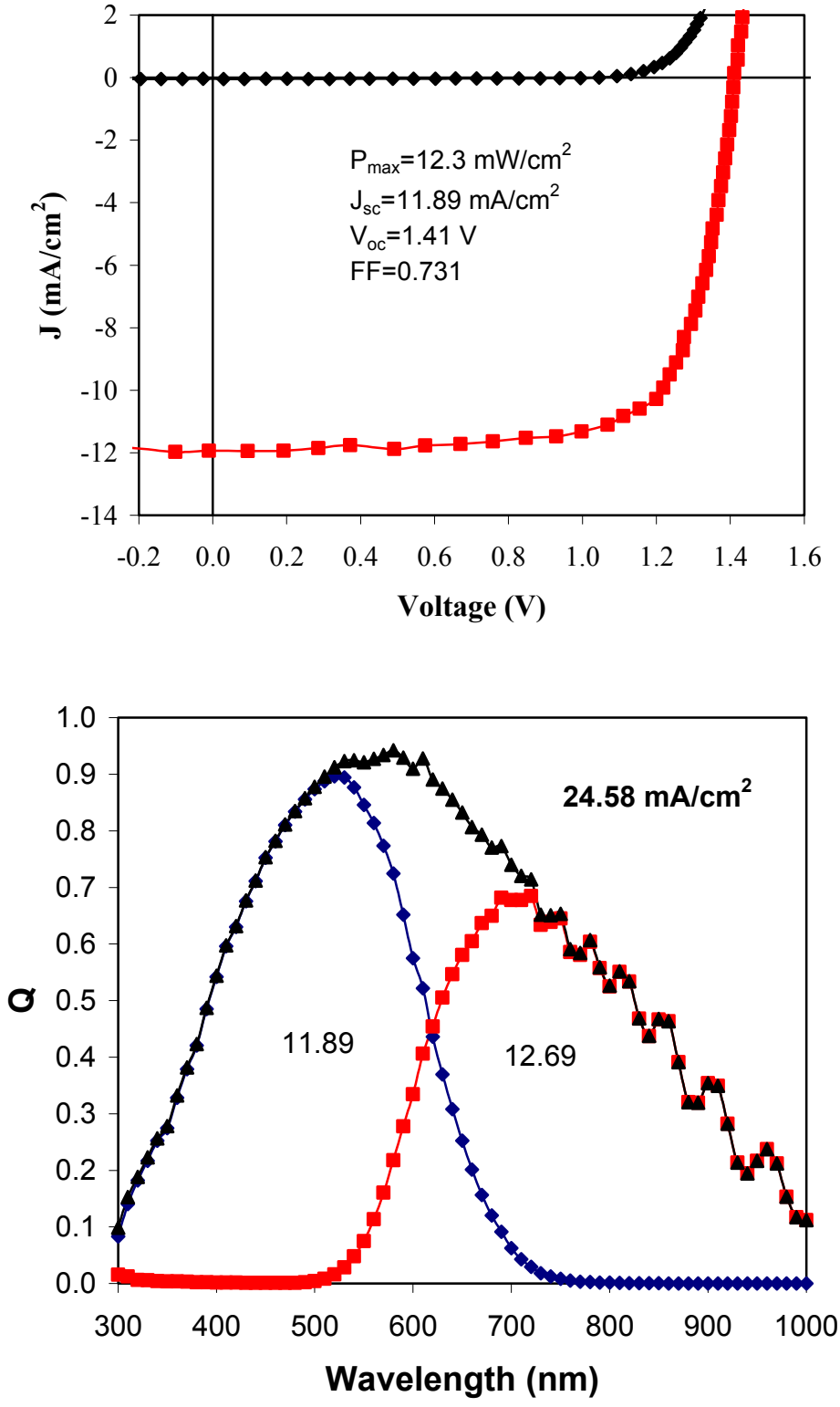

Figure 15. (upper) J-V characteristics and (bottom) quantum efficiency of an a-Si:H/nc-Si:H double-junction cell deposited using high pressure RF glow discharge at ~ 3 Å/s.

Section 6: Large-area a-Si:H/nc-Si:H Double-junction Solar Cells

6.1. Introduction

As presented in the previous sections, we have explored various techniques for nc-Si:H deposition at different rates. We have shown an initial efficiency of 13.4% with an a-Si:H/nc-Si:H double-junction cell and 14.6% with an a-Si:H/a-SiGe:H/nc-Si:H triple-junction cell with an active-area of 0.25 cm^2. In order to use the multi-junction structure with nc-Si:H in the bottom cell, an increase in the deposition rate and improvement of the deposition uniformity on large area substrates are two major issues that need to be investigated. In this section, we will present our recent progress in the development of large-area a-Si:H/nc-Si:H double-junction solar cells and modules. The main focus at this moment is to investigate the issues related to large-area deposition and module fabrication. Therefore, the primary work is limited to the low deposition rate regimes.

6.2. Experimental

nc-Si:H films and solar cells were deposited using a large-area multi-chamber RF glow discharge system (2B machine) with gas mixtures of H_2 and SiH_4 on substrates with an area of 35 × 33 cm^2. a-Si:H/nc-Si:H double-junction solar cells with an *n-i-p* structure were deposited on Ag/ZnO back reflector coated stainless steel substrates. The thicknesses of the intrinsic a-Si:H and nc-Si:H layers are about 2000-3000 Å and 1-2 μm, respectively. Indium-Tin-Oxide was deposited on top of the *p* layer as a transparent contact. Metal grids or wires were used to reduce the series resistance and improve the collection of current. The thickness uniformity was measured on different locations using an optical method, and the uniformity of cell performance was characterized by evaluating small-area cells defined by ITO dots with an active-area of 0.25 cm^2 on the *p* layer of the large-area a-Si:H/nc-Si:H double-junction cells. The current density versus voltage, J-V, characteristics were measured under an AM1.5 solar simulator at 25 °C. Quantum efficiency, QE, was measured for wavelength from 300 nm to 1000 nm. Modules with aperture areas of 45 cm^2 and 460 cm^2 were made using our conventional module fabrication procedure. The module efficiency was measured under a Spire solar simulator at 25 °C. The light soaking experiment was done under 100 mW/cm^2 of white light at 50 °C.

6.3. Uniformity of thickness and cell performance

Uniform cell performance ensures high efficiency of large-area solar cells and modules. The thickness uniformity depends on the cathode structure and deposition parameter. By incorporating an improved cathode and optimizing the deposition conditions, we have improved the thickness uniformity. The thickness non-uniformity for the nc-Si:H films is within 15% in a 30 × 30 cm^2 area and less than 10% in an area of 460 cm^2. The uniformity of cell performance was characterized by measuring the small-area cells (0.25 cm^2) defined by ITO dots at different locations over the large area deposition. Figure 15 (a) shows the distribution of the conversion efficiency of a sample across a 22 × 22 cm^2 area. The value at each position represents the

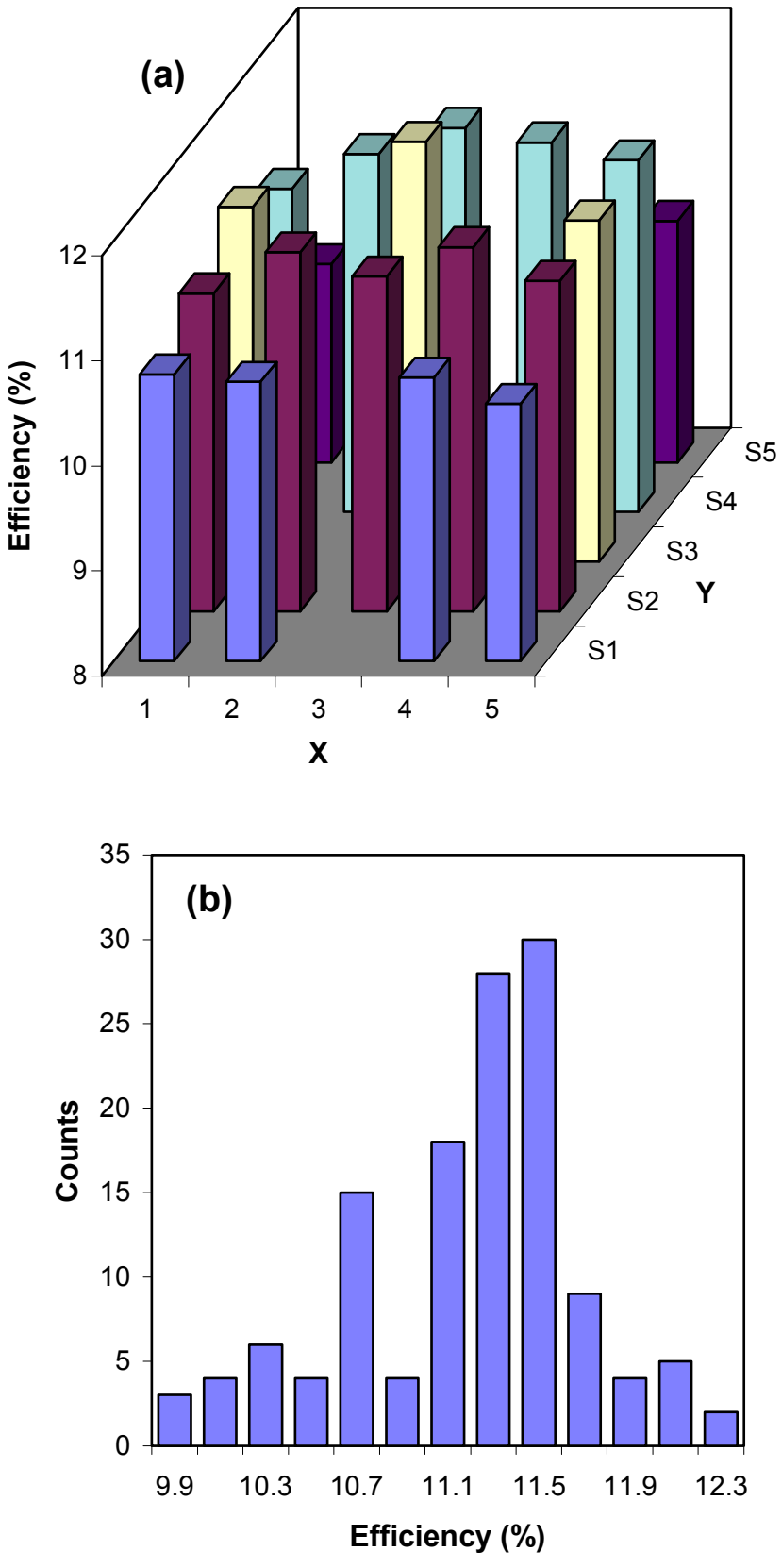

Figure 16. (a) Spatial distribution of solar cell efficiency over a large-area substrate. Each unit on the X-axis and Y-axis is about 4 cm. (b) The distribution of efficiency of sample 9504.

average efficiency of the cells with an active-area of 0.25 cm^2 on a 4 × 4 cm^2 piece. One can see that the cells with the highest efficiency are located in the center area of the substrate. The cells on the edge have lower efficiencies, whereas, the cell efficiency is the lowest at the corners. The performance non-uniformity is similar to the thickness non-uniformity. Overall, the uniformity in the central area of 460 cm^2 is acceptable for module fabrication. Figure 16 (b) shows the distribution of the efficiency for all the cells with an active-area of 0.25 cm^2. The efficiency is in the range from 10% to 12% with a peak position at ~ 11.5%. The highest efficiency after QE correction for J_{sc} is 12.1% as shown in Fig. 16.

6.4. Large-area a-Si:H/nc-Si:H double-junction modules

Several a-Si:H/nc-Si:H double-junction modules with areas of 45 and 461 cm^2 were fabricated. Figure 18 shows a picture of three modules. The best aperture-area efficiency is 11.8% for the 45 cm^2 cell and 11.3% for the 461 cm^2 one. Figure 19 shows the J-V characteristics of the two solar cells. The solar cells with a larger area of ~ 460 cm^2 were encapsulated. The results are listed in Table VIII. After encapsulation, the efficiency decreased by ~ 6-7%, which is slightly more than the loss in the conventional lamination for a-Si:H/a-SiGe:H/a-SiGe:H triple-junction cells. The loss of the efficiency is mainly due to the reduction of the short-circuit current density. The highest efficiency of the encapsulated large-area module is 10.6 %.

Table IX. J-V characteristic of the large-area modules before and after encapsulation.

Sample No.	State	Area (cm^2)	V_{oc} (V)	I_{sc} (A)	FF	P_{max} (W)	Eff. (%)
9446	Unencapsulated	462	1.409	5.304	0.694	5.191	11.23
	Encapsulated	460	1.400	4.860	0.703	4.782	10.40
9456	Unencapsulated	461	1.402	5.317	0.690	5.139	11.12
	Encapsulated	456	1.395	4.914	0.693	4.750	10.42
9461	Unencapsulated	461	1.419	5.432	0.676	5.211	11.30
	Encapsulated	458	1.408	5.008	0.688	4.849	10.59
9464	Unencapsulated	460	1.427	5.239	0.651	4.864	10.57
	Encapsulated	458	1.420	4.756	0.658	4.445	9.71

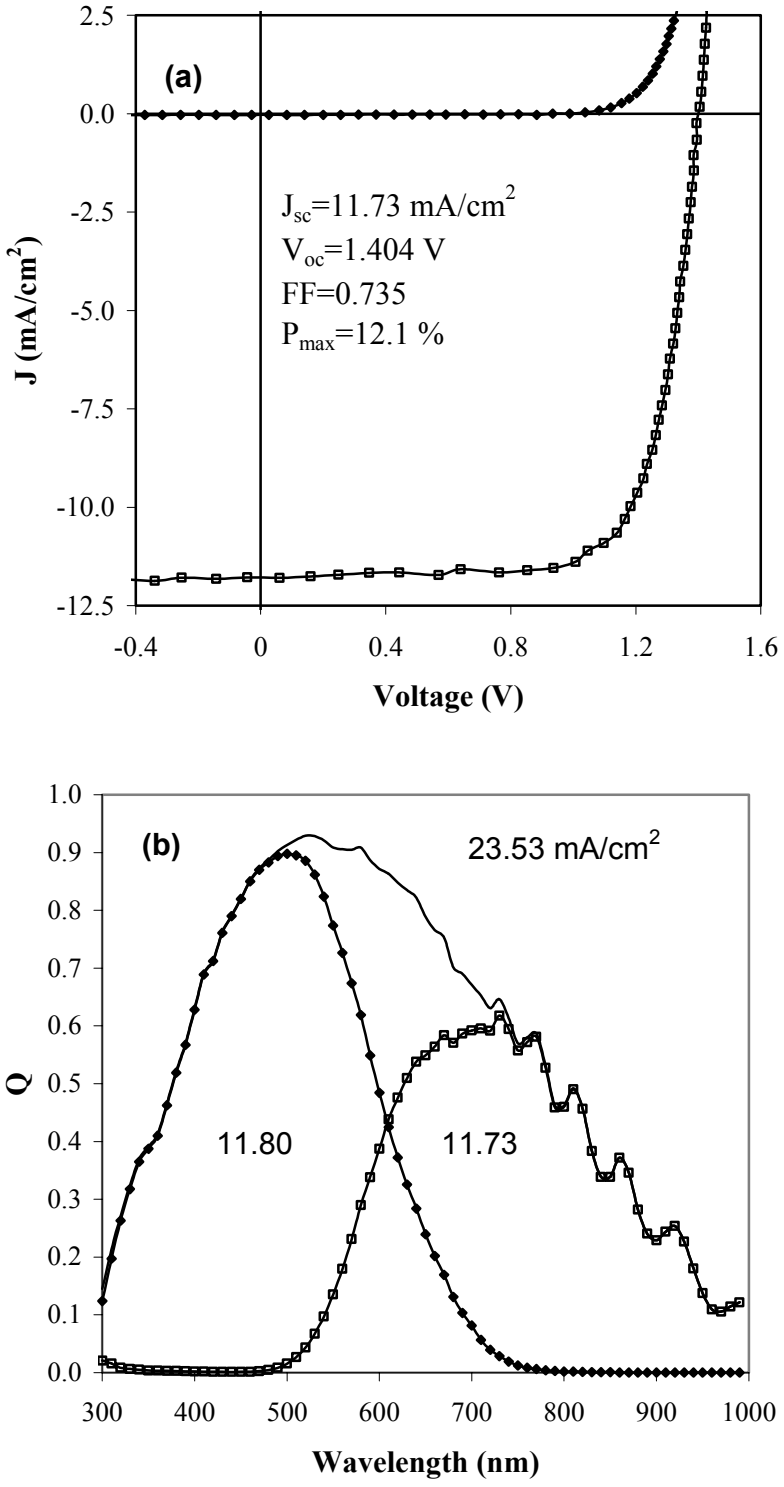

Figure 17. (a) J-V characteristics and (b) quantum efficiency of an a-Si:H/nc-Si:H double-junction solar cell.

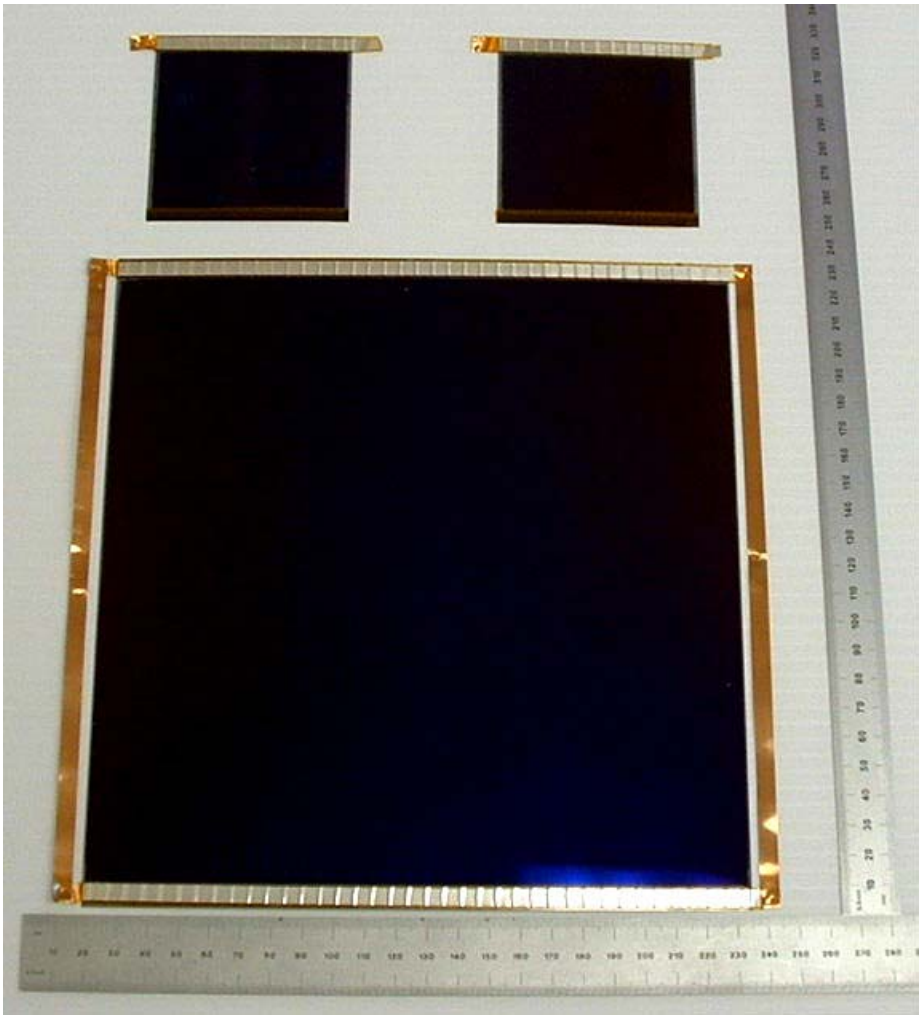

Figure 18. a-Si:H/nc-Si:H double-junction modules on textured Ag/ZnO coated stainless steel substrates with aperture areas of 45 cm^2 (top) and 461 cm^2 (bottom).

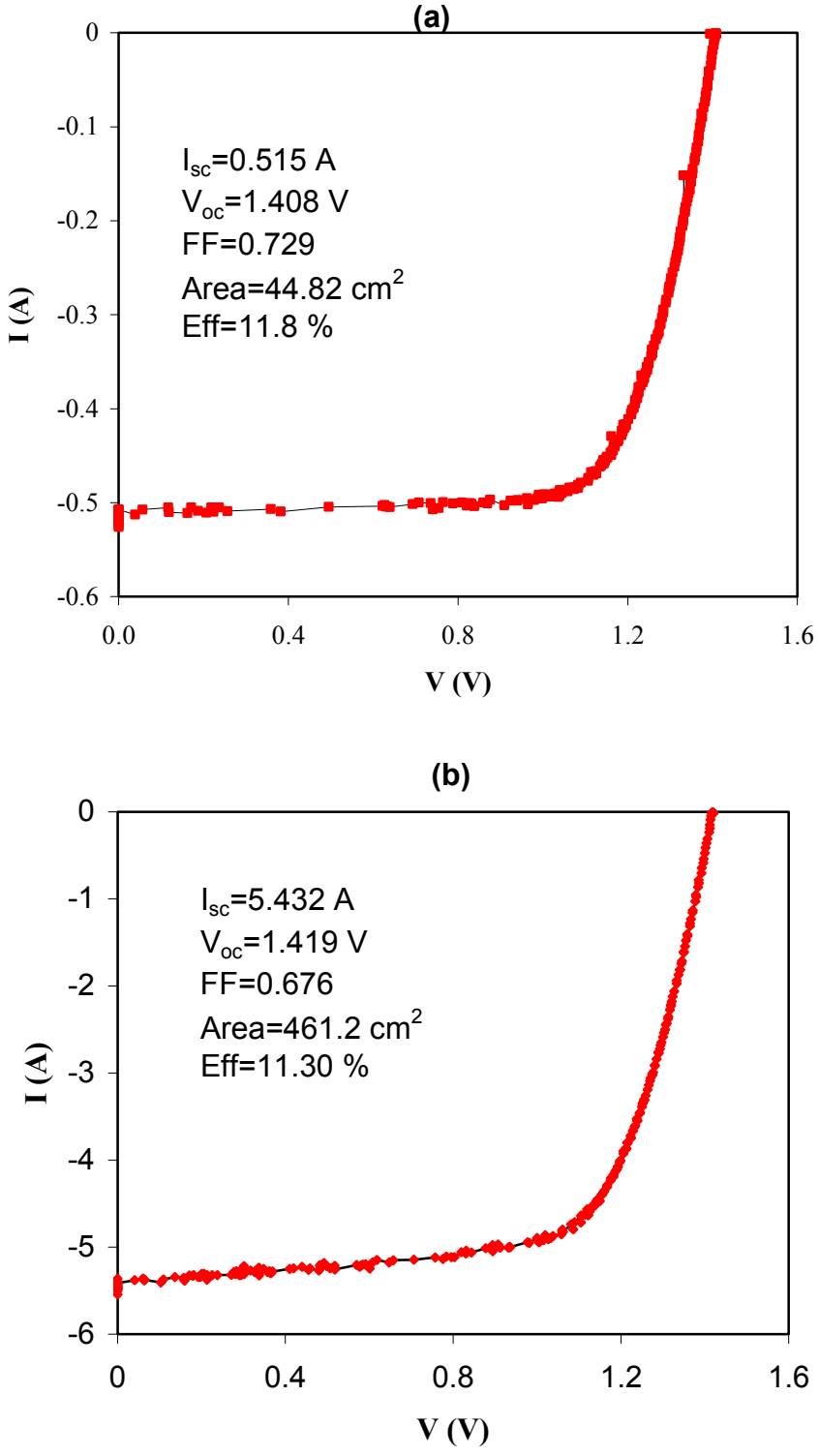

Figure 19. J-V characteristics of a-Si:H/nc-Si:H double-junction cells with aperture areas of (a) 45 cm^2 and (b) 461 cm^2.

6.5. Stability of large-area a-Si:H/nc-Si:H double-junction solar cell and module

It has been reported that nc-Si:H solar cells generally do not degrade after light soaking [4]. However, as presented in the previous sections, we find that under one sun illumination, nc-Si:H single-junction cells degrade by about 5% to 15%, depending on the deposition conditions and the cell structure. No light-induced degradation has been observed under a red light (wavelength>665 nm, see section 8) for the same cells even when a higher light intensity was used. We believe that, in general, nc-Si:H single-junction solar cells should have some light-induced degradation under white light illumination since there is always a certain amount of amorphous phase in the material. When nc-Si:H is deposited as the bottom cell in multi-junction structures or illuminated with long wavelength light, the nc-Si:H does not see much light with energy larger than the bandgap in the amorphous phase, and very little or even no light induced degradation is observed.

In the a-Si:H/nc-Si:H double-junction structure, we found that a bottom-cell limited current mismatch is desirable for stable efficiency [3]. Table X lists the stability results of three small area a-Si:H/nc-Si:H double-junction solar cells, where the stable efficiencies were obtained after light soaking under 100 mW/cm^2 of white light for over 1000 hours. For most a-Si:H/nc-Si:H double-junction cells, the light-induced degradation appears during the first 100 to 200 hours of light soaking, and then the efficiency stabilizes. It appears that the overall degradation is about 10%, which is similar to our a-Si:H/nc-Si:H tandem cells on small-area substrates. The encapsulated modules, as listed in Table IX, were also light-soaked. The results are summarized in Table XI. The degradation is in the range between 8 to 12%, similar to the results obtained from small area solar cells. The highest stabilized module efficiency is 9.5%. Measurement at NREL obtained an aperture-area efficiency of 9.2%.

6.6. Summary

We have made large-area deposition of a-Si:H/nc-Si:H double-junction solar cells using RF glow discharge at a relatively low rate ~ 1 Å/s. The thickness uniformity is well within ± 10%. The cell performance uniformity was characterized by depositing ITO dots with an active-area of 0.25 cm^2 on the *p* layer of one large-area a-Si:H/nc-Si:H double-junction cell. The small-

Table X. Stability of a-Si:H/nc-Si:H double-junction solar cells with an active area 0.25 cm^2.

Sample No.	State	V_{oc} (V)	J_{sc} (mA/cm^2)	Q (mA/cm^2)		FF	Eff. (%)
				Top	Bott.		
9701LC1	Initial	1.406	11.16	11.89	**11.16**	0.765	12.00
	Stabilized	1.377	11.16	**11.59**	11.18	0.715	11.0
	Degradation	2.06%	0%	3.2%	0.35%	6.7%	8.3%
9504LC2	Initial	1.404	11.73	11.80	**11.73**	0.735	12.10
	Stabilized	1.369	11.28	**11.28**	11.58	0.694	10.72
	Degradation	2.5 %	3.8%	4.4 %	1.3 %	5.6 %	11.4%
9511LC1	Initial	1.389	11.28	11.90	**11.28**	0.764	11.97
	Stabilized	1.356	11.17	11.59	**11.17**	0.707	10.71
	Degradation	2.4%	1.0%	2.6%	1.0%	7.5%	10.5%

Table XI. Stability of a-Si:H/nc-Si:H double-junction modules after 1050 hours of light soaking under 100 mW/cm^2 of white light at 50 ^{o}C.

Sample No.	Area (cm^2)	State	V_{oc} (V)	I_{sc} (A)	FF	P_{max} (W)	Eff. (%)
9446	460	Initial	1.400	4.860	0.703	4.782	10.40
		Stabilized	1.378	4.774	0.662	4.356	9.48
		Degradation	1.57 %	1.77 %	5.83 %	8.91 %	8.9 %
9456	456	Initial	1.395	4.914	0.693	4.750	10.42
		Stabilized	1.373	4.817	0.648	4.283	9.40
		Degradation	1.58 %	1.97 %	6.49 %	9.83 %	9.8 %
9461	458	Initial	1.408	5.008	0.688	4.849	10.59
		Stabilized	1.378	4.827	0.638	4.246	9.27
		Degradation	2.13 %	3.61 %	7.27 %	12.44 %	12.4 %
9464	458	Initial	1.420	4.756	0.658	4.445	9.71
		Stabilized	1.399	4.631	0.633	4.104	8.96
		Degradation	1.48 %	2.63 %	3.82 %	7.67 %	7.7 %

area cells showed an efficiency distribution in the range from 10% to 12% with a peak position at 11.5%. Preliminary results of large-area a-Si:H/nc-Si:H double-junction structure cells show an initial aperture-area efficiency of 11.8% and 11.3% for 45 cm^2 and 461 cm^2 size un-encapsulated solar cells, respectively. The 11.3% cell became 10.6% after encapsulation and stabilized at 9.5% after prolonged light soaking. Currently, we are working on increasing the deposition rate and reducing the nc-Si:H layer deposition time. A preliminary result shows an initial active-area efficiency of 11.3% from a high rate deposited a-Si:H/nc-Si:H double-junction cell.

Section 7: Status of a-Si:H/a-SiGe:H/a-SiGe:H Triple-junction Solar Cells Made with 30 MW Production Constraints

For a-Si:H/a-SiGe:H/a-SiGe:H triple-junction solar cells with production constraints, we have achieved an initial efficiency of 11.23%. This result was achieved with (i) a cathode design that resembles the one on the production line; (ii) a back reflector obtained from the production line and (iii) a SiH_4 and GeH_4 mixture instead of a Si_2H_6 and GeH_4 mixture. Table XII lists the individual solar cell parameters in the initial and stable (100 mW/cm^2) white light illumination for 1070 hours) states. The overall degradation loss is seen to be 12.5% comprising losses in FF (6.9%), V_{oc} (4.2%) and J_{sc} (1.3%). The stable active area efficiency is 9.8%. This corresponds to a stable total area efficiency of 9.1% and ties with the previous record made with a Si_2H_6 and GeH_4 mixture. Figure 20 shows the (a) J-V characteristics and (b) quantum efficiency of this solar cell.

Table XII. The initial and stable performance of the a-Si:H/a-SiGe:H/a-SiGe:H triple cell deposited under production constraints.

Run No.	State	V_{oc} (V)	FF	J_{sc} (mA/cm^2)	QE (mA/cm^2)				P_{max} (mW/cm^2)
					Top	Mid.	Bot.	Total	
9619 S	Initial	2.198	0.736	6.94	7.19	7.55	6.94	21.69	11.23
	Stable	2.104	0.682	6.85	7.07	7.29	6.85	21.20	9.83
	Degr.	4.23%	6.93%	1.3%	1.67%	3.44%	1.3%	2.26%	12.5%

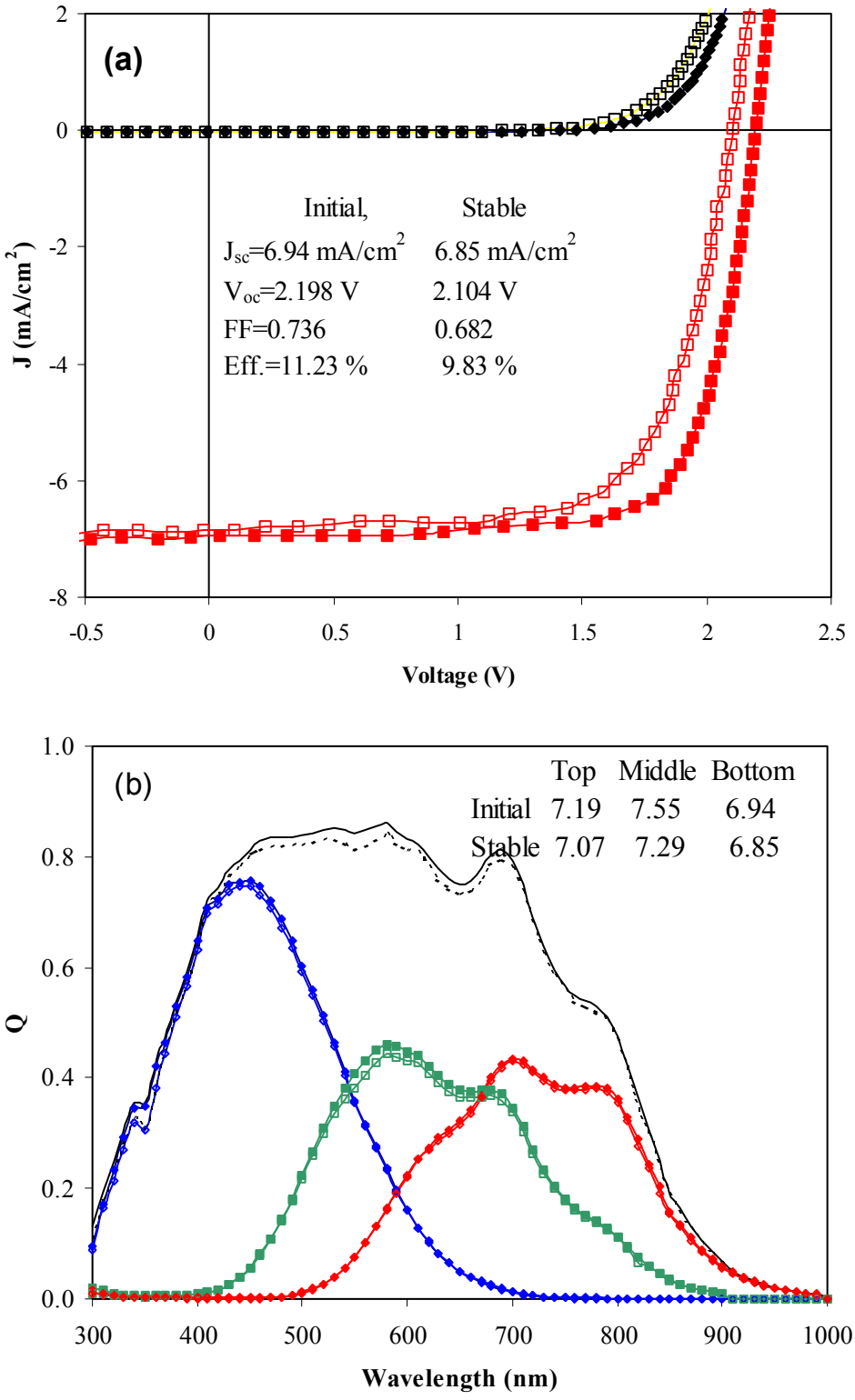

Figure 20. (a) J-V characteristic and (b) quantum efficiency of an a-Si:H/a-SiGe:H/a-SiGe:H triple-junction solar cell before and after 1000 hours of light soaking.

Section 8: Metastability of nc-Si:H Solar Cells

8.1. Introduction

The Staebler-Wronski effect has limited the development of a-Si:H solar cells. Although significant amount of work has been carried out in the last twenty-five years, an effective way has not been developed to eliminate the light-induced degradation in a-Si:H based solar cells. As an alternative material, nc-Si:H has attracted remarkable attention. One advantage of using nc-Si:H in thin film solar cells is its better stability under prolonged light soaking than a-Si:H and a-SiGe:H alloys. It has generally been reported that no light-induced degradation was observed in nc-Si:H solar cells. However, the term nc-Si:H represents a wide range of materials comprised of various grain sizes and different microcrystalline volume fractions. The highest efficiency nc-Si:H solar cells are normally deposited near the transition from nanocrystalline to the amorphous phase, which means a large amount of amorphous phase still exists in the nc-Si:H materials. Therefore, it would be logical to assume light-induced degradation in nc-Si:H solar cells deposited in this regime. Indeed, Finger and his colleagues found that nc-Si:H solar cells made with a hydrogen dilution close to the transition show light induced degradation. The amount of degradation depends on the dilution ratio, hence, on the microcrystalline volume fraction and grain size. [15]

In general, nc-Si:H can be considered a two-phase material with nanocrystallites surrounded by amorphous tissue. The photons with energy higher than the bandgap of a-Si:H are largely absorbed in the amorphous phase while the lower energy photons are absorbed in the grains. Since the material properties inside the grains would be similar to crystalline silicon with no light induced defects, one may expect no light induced defect generation in nc-Si:H when it is exposed to red light with photon energy lower than the optical bandgap of a-Si:H. If this hypothesis is correct, there would be much less light induced degradation in the nc-Si:H bottom cell in an a-Si:H/nc-Si:H double-junction structure, because the high-energy photons are absorbed in the a-Si:H top cell.

8.2. Experimental

Systematically, we have studied the light induced degradation of nc-Si:H single-junction solar cells with various light sources. Two sets of nc-Si:H single-junction solar cells were studied. The cells in each set were from one run of deposition on the same substrate; and therefore, the cell performance is very similar. One set was deposited using MVHF at a high rate with relatively low V_{oc}. The other set was deposited with RF at a low rate with relatively high V_{oc}. We believe that the RF cells have a lower microcrystalline volume fraction than the MVHF cells. As a comparison, we also studied a set of a-SiGe:H bottom cells. Light soaking was done at 25 °C under open circuit condition. An AM1.5 solar simulator was used as the light source. Focus lenses and filters were used to vary the light intensity and the spectrum. The current density versus voltage (J-V) characteristics were measured as a function of light soaking time under the same light used for the light soaking. The light soaking time was 15 hours. The J-V characteristics in the initial state and degraded state after light soaking were measured under an AM1.5 illumination and by quantum efficiency measurement. Due to the difference in responses for different wavelengths, we used the same photo-generated carrier density for different light

spectra. We have found that for solar cells with a good FF, J_{sc} is a reasonable measure of the photo-carrier density. Thus, we adjusted the light intensities for different spectra to produce the same initial J_{sc} value. Here, two J_{sc} values were chosen: one is the same as the J_{sc} under AM1.5 illumination, and the other is double the value under AM1.5.

8.3. Results and Discussion

Figure 21 shows a comparison of the normalized maximum power, P_{max}, as a function of light soaking time for the MVHF nc-Si:H single-junction solar cell and the a-SiGe:H single-junction bottom cell, where the red and blue lights were obtained using a 665 nm long-pass filter and a 650 nm short-pass filter. The long-pass filter only allows the photons with energy lower than 1.86 eV, smaller than the optical bandgap of a-Si:H, to pass through and illuminate the sample. For the nc-Si:H cell, the light intensities were adjusted to produce a J_{sc}~44 mA/cm^2, approximately twice the J_{sc} under AM1.5 illumination, for the white, red, and blue lights. For the a-SiGe:H cell, the light intensities were adjusted to produce a J_{sc}~46 mA/cm^2 with the same consideration. The figure clearly shows that there is no detectable light-induced degradation for the nc-Si:H cell under the red light, some degradation under the white light, and more degradation under the blue light.

Table XIII shows a comparison of the initial and degraded performance for five MVHF deposited nc-Si:H cells. The first two cells were light-soaked under light intensities that produced the same J_{sc} as under AM1.5. Cell 1 and cell 2 were under the white light and the red light, respectively. Notice that no light induced degradation was found in cell 2 under the red

Table XIII. Summary of the light soaking results for the nc-Si:H single junction solar cells made with MVHF at a high rate. The red light was obtained by a focused white light with a 665 nm long-pass filter, and the blue light with a 650 nm short-pass filter.

Cell No.	State	J_{sc} (mA/cm^2)	V_{oc} (V)	FF	P_{max} (mW/cm^2)	Light source
1	Initial	22.02	0.475	0.624	6.53	White (AM1.5) J_{sc}~22 mA/cm^2
	Light soaked	21.82	0.474	0.608	6.29	
	Degradation	0.91 %	0 %	2.56 %	3.68 %	
2	Initial	21.86	0.481	0.623	6.55	Red light with J_{sc}~22 mA/cm^2
	Light soaked	21.86	0.480	0.623	6.55	
	Degradation	0 %	0 %	0 %	0 %	
3	Initial	22.20	0.474	0.621	6.53	White light with J_{sc}~44 mA/cm^2
	Light soaked	22.00	0.467	0.598	6.14	
	Degradation	0.9 %	1.48 %	3.70 %	5.97 %	
4	Initial	22.19	0.472	0.620	6.49	Red light with J_{sc}~44 mA/cm^2
	Light soaked	22.11	0.473	0.619	6.47	
	Degradation	0.36 %	0 %	0 %	0.31 %	
5	Initial	21.98	0.476	0.621	6.50	Blue light with J_{sc}~44 mA/cm^2
	Light soaked	21.78	0.469	0.591	6.04	
	Degradation	0.91 %	1.47 %	4.83 %	7.08 %	

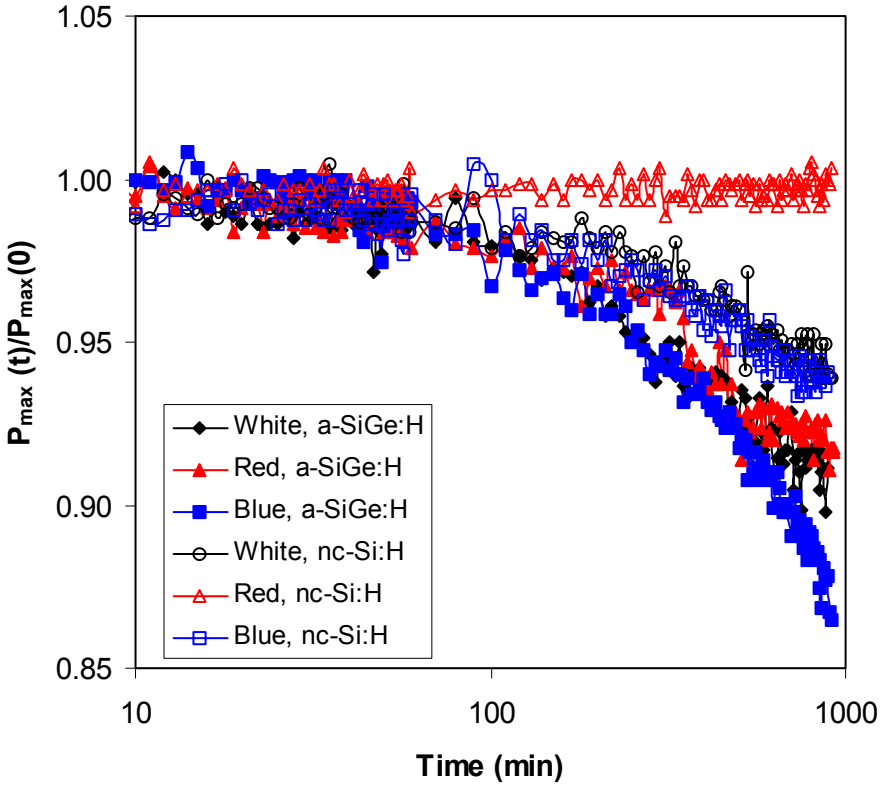

Figure 21. Light soaking kinetics of normalized efficiency of a nc-Si:H single-junction solar cell and an a-SiGe:H single-junction solar cell.

light, but it was 3.7% under the white light. To enhance the light soaking effect, we increased the light intensities to produce 44 mA/cm^2, which is twice the J_{sc} under AM1.5 illumination. There is still no detectable degradation under the red light within the experimental errors.

As discussed above, the undetectable light induced degradation under the red light is due to very little absorption in the amorphous phase, while the absorption in the microcrystalline phase does not produce defects. Two mechanisms could explain the difference between the white and blue light soaking. First, the blue light has a large portion absorbed in the amorphous phase, which produces more defects. For the white light, the portion of red light is mainly absorbed in the microcrystalline phase and does not produce degradation. Second, more blue light is absorbed nearer the *i/p* interface than in the bulk. Guha *et al.* showed that the *i/p* junction is the dominant junction and any changes in the dominant junction can cause noticeable changes in the cell performance [16].

Table XIV lists the J-V characteristics at the initial and degraded states for three RF deposited solar cells. The general trend is the same as the MVHF deposited cells, i.e., the red light produces low degradation, the white light some degradation, and the blue light more degradation. However, unlike the MVHF cell, this cell still has 2.2% degradation under the red light. We believe that the difference could be caused by the different material structure. For the RF deposited cells, the V_{oc} is larger than the MVHF deposited ones. It could indicate that there is more amorphous component in the RF cells than in the MVHF cells, which may partially play a role in the light-induced degradation. Although the cut-on filter with a wavelength longer than 665 nm blocks most of the high energy photons, there are still some photons absorbed by the amorphous tissue, which degrades the cell performance.

Table XV summarizes the results of the a-SiGe:H bottom cells. For the a-SiGe:H cell, the material is homogeneous, and only one optical bandgap is defined with a value around 1.4 eV. The differences among the light soaked samples under the lights with the three spectra are mainly due to the second mechanism (dominant junction effect) discussed above. Overall, the light-induced degradation in the nc-Si:H cell is much less than that in the a-SiGe:H cell even

Table XIV. Summary of the light soaking results for the nc-Si:H single junction solar cells made with RF at a low rate. These cells have a high V_{oc} and probably a high amorphous component in the intrinsic layer. The red light was a focused white light with a 665 nm long-pass filter and the blue light with a 650 nm short-pass filter.

Cell No.	State	Q (mA/cm^2)	V_{oc} (V)	FF	P_{max} (mW/cm^2)	Light source
1	Initial	24.43	0.525	0.596	7.64	White light with J_{sc}~48 mA/cm^2
	Light soaked	23.86	0.521	0.578	7.51	
	Degradation	1.80 %	0.76 %	3.02 %	5.89 %	
2	Initial	24.42	0.526	0.598	7.68	Red light with J_{sc}~48 mA/cm^2
	Light soaked	24.22	0.523	0.593	7.51	
	Degradation	0.82 %	0.57 %	0.84 %	2.20 %	
3	Initial	24.28	0.525	0.605	7.71	Blue light with J_{sc}~48 mA/cm^2
	Light soaked	23.80	0.521	0.580	7.19	
	Degradation	1.98 %	4.83 %	5.77 %	7.23 %	

under white and blue light sources. We need to point out that the light-soaked state is not a stabilized state since only a 15-hour light soaking was performed.

The above experiment confirms no or very little light-induced degradation for nc-Si:H solar cells under red light with photon energy lower than the bandgap of a-Si:H. In an a-Si:H/nc-Si:H double-junction solar cell, most blue light is absorbed by the a-Si:H top cell, and the nc-Si:H bottom cell only absorbs red light with low photon energy. Therefore, there is very little light-induced degradation in the nc-Si:H bottom cell in multi-junction structures, and a bottom cell limited current mismatching is desirable for stable efficiency as shown above and in the previous reports.

8.4. Summary

We have systematically studied the light-induced degradation in nc-Si:H single-junction solar cells under various light soaking conditions. We found no detectable degradation under red light with photon energies less than the bandgap of a-Si:H. We believe that the low energy photons are only absorbed in the microcrystalline phase, where no light induced defect generation occurs. Under white and blue lights, the defect generation in the amorphous phase causes certain degradation. The fact that a larger degradation is observed under blue light than white light is due to more absorption in the amorphous phase and more absorption near the *i/p* interface under blue light than under white light. These results provide an explanation that a bottom cell limited-current mismatch in multi-junction structures with nc-Si:H as the bottom cell leads to a high stable efficiency.

Table XV. Summary of the light soaking results for the a-SiGe:H bottom single-junction solar cells. The red light was a focused white light with a 665 nm long-pass filter, and the blue light with a 650 nm short-pass filter.

Cell No.	State	J_{sc} (mA/cm^2)	V_{oc} (V)	FF	P_{max} (mW/cm^2)	Light source
1	Initial	23.40	0.624	0.575	8.40	White light with J_{sc}~23 mA/cm^2 (AM 1.5)
	Light soaked	22.94	0.608	0.563	7.85	
	Degradation	1.97%	2.56%	2.09%	6.55%	
2	Initial	23.10	0.628	0.601	8.72	White light with J_{sc}~46 mA/cm^2
	Light soaked	22.88	0.601	0.567	7.80	
	Degradation	0.95 %	4.30 %	5.66 %	10.55 %	
3	Initial	23.91	0.614	0.587	8.62	Red light with J_{sc}~46 mA/cm^2
	Light soaked	23.48	0.601	0.563	7.94	
	Degradation	1.80 %	2.12 %	4.09 %	7.89 %	
4	Initial	23.50	0.621	0.572	8.35	Blue light with J_{sc}~46 mA/cm^2
	Light soaked	22.91	0.591	0.539	7.30	
	Degradation	2.51 %	4.83 %	5.77 %	12.57 %	

Section 9: Future Work

We have made significant progress during the Phase II of this program. We will continue our efforts in the Third Phase to accomplish the milestones. The main focuses for phase III are summarized below.

9.1. High efficiency multi-junction solar cells

To achieve an even higher efficiency, we need to increase the total photocurrent density. Currently, we have achieved a total photocurrent density around 26-27 mA/cm^2. This value is significantly higher than the record set in Phase I, but it is still not as high as reported in the literature [1][2]. If we obtain a total photocurrent density of over 30 mA/cm^2, we shall achieve an initial active-area efficiency larger than 16% (J_{sc}=9.6 mA/cm^2, V_{oc}=2.2 V, FF=0.76) and consequently improve the stable efficiency. To achieve this goal, we continue to optimize the nc-Si:H bottom cell by optimizing the deposition conditions and cell design. At the same time, we will optimize the back reflector.

9.2. High rate deposition of multi-junction solar cells

For high rate deposition, we will continue to work on the MVHF deposition. Two major issues need to be addressed. First, we shall increase the deposition rate further to limit the nc-Si:H intrinsic layer deposition time less than 30 minutes. Second, we shall improve the cell performance further. In Phase II, 11.0% and an 11.4% stable active-area efficiencies have been achieved using an a-Si:H/nc-Si:H double-junction and an a-Si:H/a-SiGe:H/nc-Si:H triple-junction structure. These results were obtained by using a flat hydrogen dilution profile. As shown in Section 2, hydrogen dilution profiling is a very effective method to improve nc-Si:H solar cell performance; and we shall use the same method in the high rate deposition.

RF glow discharge under a high pressure depleting regime show very promising results in nc-Si:H solar cell deposition. We shall continue to optimize the deposition condition to improve cell performance and uniformity. In the interim, we shall increase the deposition rate and reduce the deposition time. We are targeting for a deposition time of 30 minutes.

We shall compare the advantages and disadvantages between MVHF and the high pressure RF deposition of nc-Si:H solar cells.

9.3. Explore new deposition regime for a-SiGe:H alloy

The big breakthrough for a-Si:H and a-SiGe:H alloys in solar cell applications is high hydrogen dilution, which improves not only the efficiency but also the stability under light soaking. Most of the deposition parameters in the current deposition regime have been tested. Although the a-SiGe:H quality has been improved through the constant studies in the program, the narrow bandgap a-SiGe:H bottom cell is still the bottleneck for high efficiency multi-junction solar cells. In order to obtain even higher efficiency, we need to explore some new deposition conditions such as a high pressure RF glow discharge. For this purpose, systematic studies on the plasma physics and chemistry would be helpful.

9.4. Optimization of a-Si:H/a-SiGe:H/a-SiGe:H triple-junction cells and modules

Our 2B machine has been upgraded. As a result, the uniformity has been improved significantly. In Phase II, we have worked on the optimization of component cells and triple-junction cells using SiH_4 as a substitute for Si_2H_6 in the a-SiGe:H alloy. We achieved similar results to the record achieved by using Si_2H_6. In Phase III, we shall work on the large-area a-Si:H/a-SiGe:H/a-SiGe:H triple-junction modules to accomplish the proposed milestones. Meanwhile, we will modify the geometry of the reactor based on the new understanding to minimize the light-induced degradation and achieve higher efficiency.

REFERENCES

[1] K. Yamamoto, A. Nakajima, M. Yoshimi, T. Sawada, S. Fukuda, T. Suezaki, M. Ichikawa, Y. Koi, M. Goto, H. Takata, T. Sasaki, and Y. Tawada, *Proc. of 3rd World Conf. on Photovoltaic Energy Conversion* (May 2003, Osaka, Japan), p. 2789.

[2] K. Saito, M. Sano, H. Otoshi, A. Sakai, S. Okabe, and K. Ogawa, *Proc. of 3rd World Conf. on Photovoltaic Energy Conversion* (May 2003, Osaka, Japan), p. 2793.

[3] B. Yan, G. Yue, J. Yang, A. Banerjee, and S. Guha, *Mater. Res. Soc. Symp. Proc.* **762**, 309 (2003).

[4] E.V. Shah, J. Meier, E. Vallat-Sauvain, N. Wyrsch, U. Kroll, C. Droz, and U. Graf, Solar Energy Materials & Solar Cells **78**, 469 (2003).

[5] Y. Nasuno, M. Kondo, and A. Matsuda, *Proc. of 28th IEEE Photovoltaic Specialists Conference* (IEEE, Anchorage, Alaska, 2000), p.142.

[6] M. Kondo, Solar Energy Materials & Solar Cells, **78**, 543 (2003).

[7] F. Finger, S. Klein, T. Dylla, A. L. Baia Neto, O. Vetterl, and R. Carius, *Mater. Res. Soc. Symp. Proc.* **715**, 123 (2002).

[8] B. Rech, J. Muller, T. Repmann, O. Kluth, T. Roschek, J. Hupkes, H. Stiebig, and W. Appenzeller, *Mater. Res. Soc. Symp. Proc.* **762**, 285 (2003).

[9] J. Kočk, H. Stuchlíková, J. Stuchlík, B. Rezek, T. Mates, and A. Fejfar, Technical Digest of the International PVSEC-12, (Jeju, Korea, 2001) p. 469.

[10] J. Kočk, A. Fejfar, H. Stuchlíková, J. Stuchlík, P. Fojtík, T. Mates, B. Rezek, K. Luterová, V. Šverčk, and I. Pelant, Solar Energy Material & Solar Cells, **78** 493 (2003).

[11] S. Guha, J. Yang, D. L. Williamson, Y. Lubianiker, J. D. Cohen, and A. H. Mahan, Appl. Phys. Lett. **74**, 1860 (1999).

[12] J. Yang, A. Banerjee, and S. Guha, Appl. Phys. Lett. **70**, 2975 (1997).

[13] D. L. Williamson, Solar Energy Material & Solar Cells, **78** 41(2003).

[14] L. Guo, M. Kondo, M. Fukawa, K. Saitoh, A. Matsuda, Jpn. J. Appl. Phys. 37, L1116 (1998).

[15] S. Klein, F. Finger, R. Carius, T. Dylla, B. Rech, M. Grimm, L. Houben, and M. J. Stutzmann, *Proceeding of 2nd International Conference on Cat-CVD (Hot-Wire CVD) Process*, (Denver, Colorado, Sep. 2002), p. 202.

[16] A. Pawlikiewicz and S. Guha, *Mater. Res. Soc. Symp. Proc.* **118**, 599 (1988).